Meteorological Model Performance for Annual 2011 WRF v3.4 Simulation

1. INTRODUCTION

The Weather Research and Forecasting model (WRF) was applied for the entire year of 2011 to generate meteorological data to support emissions and photochemical modeling applications for this year. The WRF meteorological fields will be converted to air quality modeling input data and used to support assessments of ozone, PM2.5, visibility, and a variety of toxics.

The WRF model was applied to a 36 km continental United States scale domain (36US) and a 12 km continental United States scale domain (12US2). Both model simulations were initialized directly from meteorological analysis data. Model parameterizations and options outlined in this document were chosen based on a series of sensitivity runs performed by U.S. Environmental Protection Agency (USEPA) Office of Research and Development that provided an optimal configuration based on temperature, mixing ratio, and wind field. All WRF simulations were done by Computer Sciences Corporation (CSC) under contract to the USEPA.

2. MODEL CONFIGURATION

2.1 Configuration of the 36US Domain

Version 3.4 of the WRF model, Advanced Research WRF (ARW) core (Skamarock, 2008) was used for generating the 2011 simulations[1]. Selected physics options include Pleim-Xiu land surface model, Asymmetric Convective Model version 2 planetary boundary layer scheme, Kain-Fritsch cumulus parameterization utilizing the moisture-advection trigger (Ma and Tan, 2009), Morrison double moment microphysics, and RRTMG longwave and shortwave radiation schemes (Gilliam and Pleim, 2010).

The WRF model was initialized using the 12km North American Model (12NAM) analysis product provided by National Climatic Data Center (NCDC). Where 12NAM data was unavailable, the 40km Eta Data Assimilation System (EDAS) analysis (ds609.2) from the National Center for Atmospheric Research (NCAR) was used. Analysis nudging for temperature, wind, and moisture was applied above the boundary layer only. The model simulations were conducted in 5.5 day blocks with soil moisture and temperature carried from one block to the next via the ipxwrf program (Gilliam and Pleim, 2010). Landuse and land cover data were based on the 1992-1993 U.S. Geological Survey (USGS) data.

Figure 2.1 shows the 36US domain, which utilizes a Lambert conformal projection centered at (-97,40) with true latitudes of 33 and 45 degrees north. The domain contains 164 cells in the X direction and 128 cells in the Y direction. All cells are 36 km^2. As shown in Table 2.1, the

[1] Version 3.4 was the most current version of WRF at the time the 2011 meteorological model simulations were performed.

atmosphere is resolved with 35 vertical layers up to 50 mb, with the thinnest layers being nearest the surface to better resolve the planetary boundary layer (PBL).

WRF Layer	Height (m)	Pressure (mb)	Sigma
35	17,556	5000	0.000
34	14,780	9750	0.050
33	12,822	14500	0.100
32	11,282	19250	0.150
31	10,002	24000	0.200
30	8,901	28750	0.250
29	7,932	33500	0.300
28	7,064	38250	0.350
27	6,275	43000	0.400
26	5,553	47750	0.450
25	4,885	52500	0.500
24	4,264	57250	0.550
23	3,683	62000	0.600
22	3,136	66750	0.650
21	2,619	71500	0.700
20	2,226	75300	0.740
19	1,941	78150	0.770
18	1,665	81000	0.800
17	1,485	82900	0.820
16	1,308	84800	0.840
15	1,134	86700	0.860
14	964	88600	0.880
13	797	90500	0.900
12	714	91450	0.910
11	632	92400	0.920
10	551	93350	0.930
9	470	94300	0.940
8	390	95250	0.950
7	311	96200	0.960
6	232	97150	0.970
5	154	98100	0.980
4	115	98575	0.985
3	77	99050	0.990
2	38	99525	0.995
1	19	99763	0.9975
Surface	0	100000	1.000

Table 2.1 WRF layers and their approximate height above ground level.

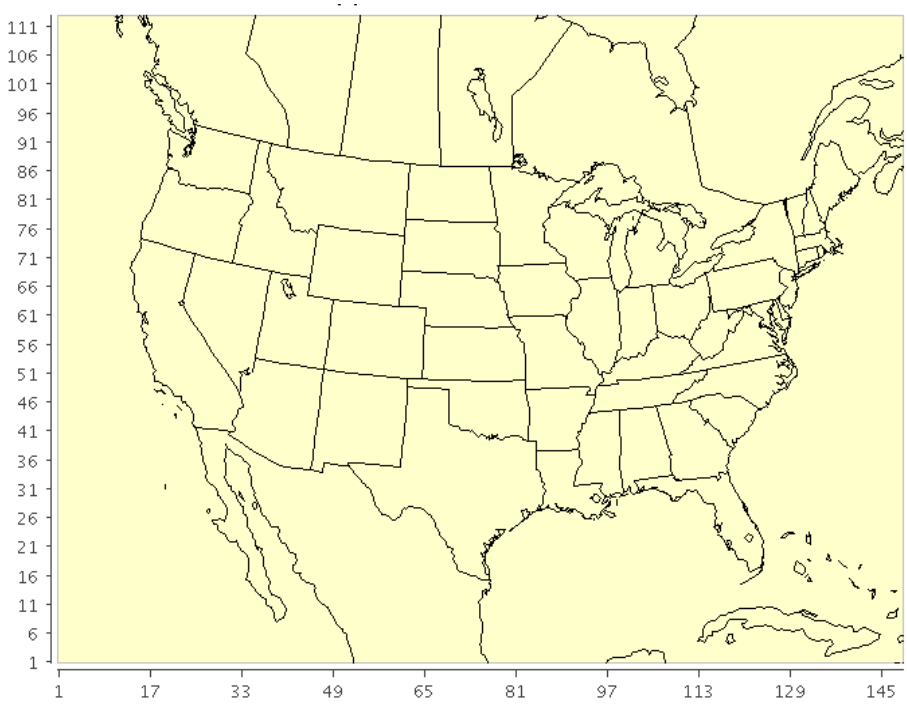

Figure 2.1 Map of WRF model domain: 36US

2.2 Configuration of the 12US2 Domain

The 12km configuration is the same as the 36km domain with two exceptions: the Group for High Resolution Sea Surface Temperatures (GHRSST) (Stammer et al., 2003) 1km SST data was used to provide more resolved information compared to the more coarse data in the NAM analysis. Additionally, landuse and land cover data were based on the National Land Cover Database 2006 (NLCD 2006). Analysis nudging for temperature, wind, and moisture was applied above the boundary layer only. The model simulations were conducted in 5.5 day blocks with soil moisture and temperature carried from one block to the next via the **ipxwrf** program (Gilliam and Pleim, 2010).

Figure 2.2 shows the 12US2 domain, which utilizes a Lambert conformal projection centered at (-97,40) with true latitudes of 33 and 45 degrees north. The domain contains 396 cells in the X direction and 246 cells in the Y direction. All cells are 12 km^2. The atmosphere is resolved with 35 vertical layers up to 50 mb (see table 2.1), with the thinnest layers being nearest the surface to better resolve the PBL.

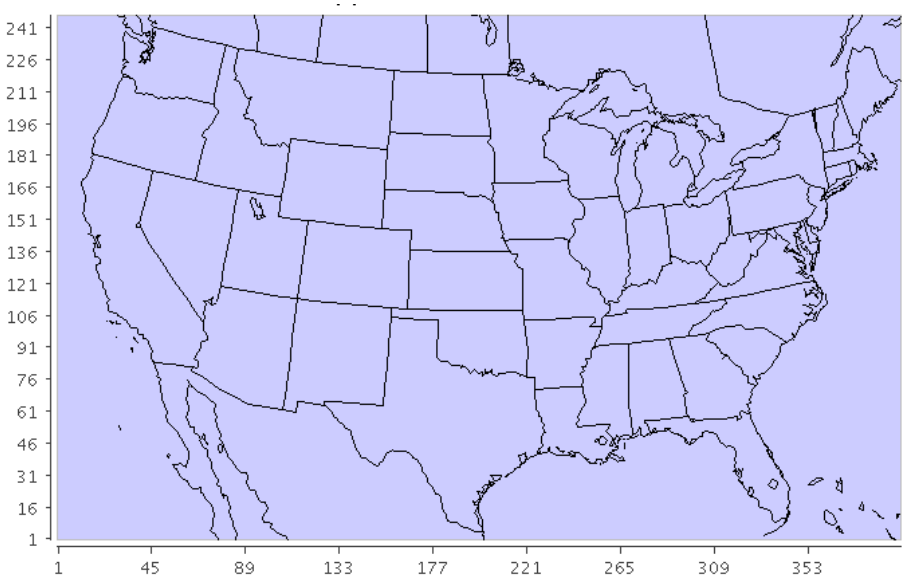

Figure 2.2 Map of WRF model domain: 12US2.

3 MODEL PERFORMANCE DESCRIPTION

The WRF model simulations were evaluated to determine whether the output fields represent a reasonable approximation of the actual meteorology that occurred during the modeling period. Identifying and quantifying these output fields allows for a downstream assessment of how the air quality modeling results are impacted by the meteorological data. For the purposes of this assessment, 2-meter temperature and mixing ratio, 10-meter wind speed and direction, and shortwave radiation are quantitatively evaluated. A qualitative evaluation of precipitation is also provided.

The observation database for surface-based temperature, wind speed and direction, and mixing ratio is based on measurements made at United States (i.e., National Weather Service) and Canadian (i.e., Environment Canada) airports. The observational dataset (ds472 network) is available from NCAR. Monitors used for evaluation are shown in Figure 3.1.

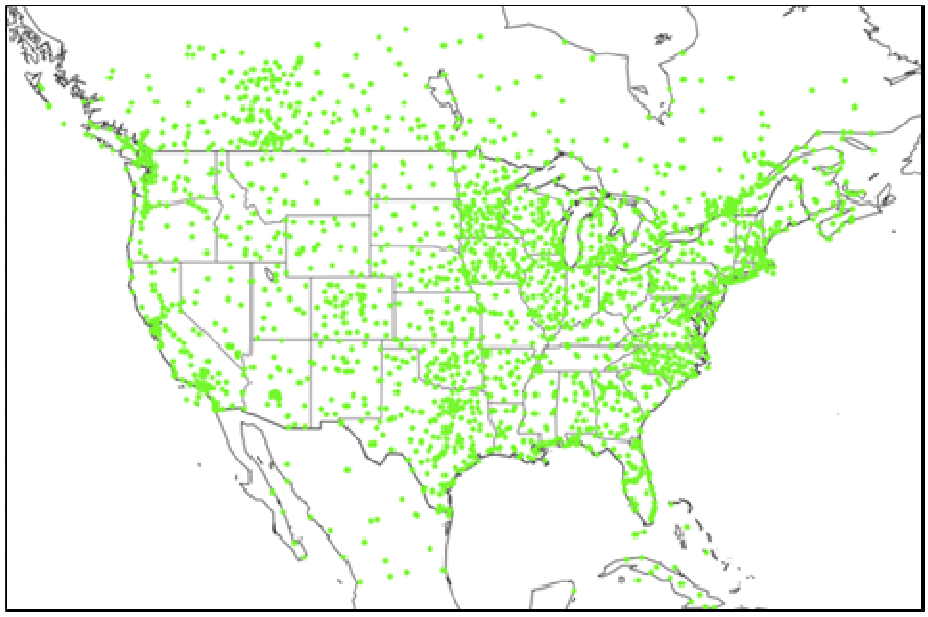

Figure 3.1 Stations used for model performance: ds472 network.

Shortwave downward radiation measurements are taken at Surface Radiation Budget Network (SURFRAD) (http://www.srrb.noaa.gov/surfrad) and Integrated Surface Irradiance Study (ISIS) (http://www.srrb.noaa.gov/isis/index.html) monitor locations. The SURFRAD network consists of 7 sites and the ISIS network consists of 9 sites across the United States (see Figure 3.2). Both networks are operated by the National Oceanic and Atmospheric Administration (NOAA), with SURFRAD sites existing as a subset of ISIS monitors that provide higher level radiation information not used in this evaluation.

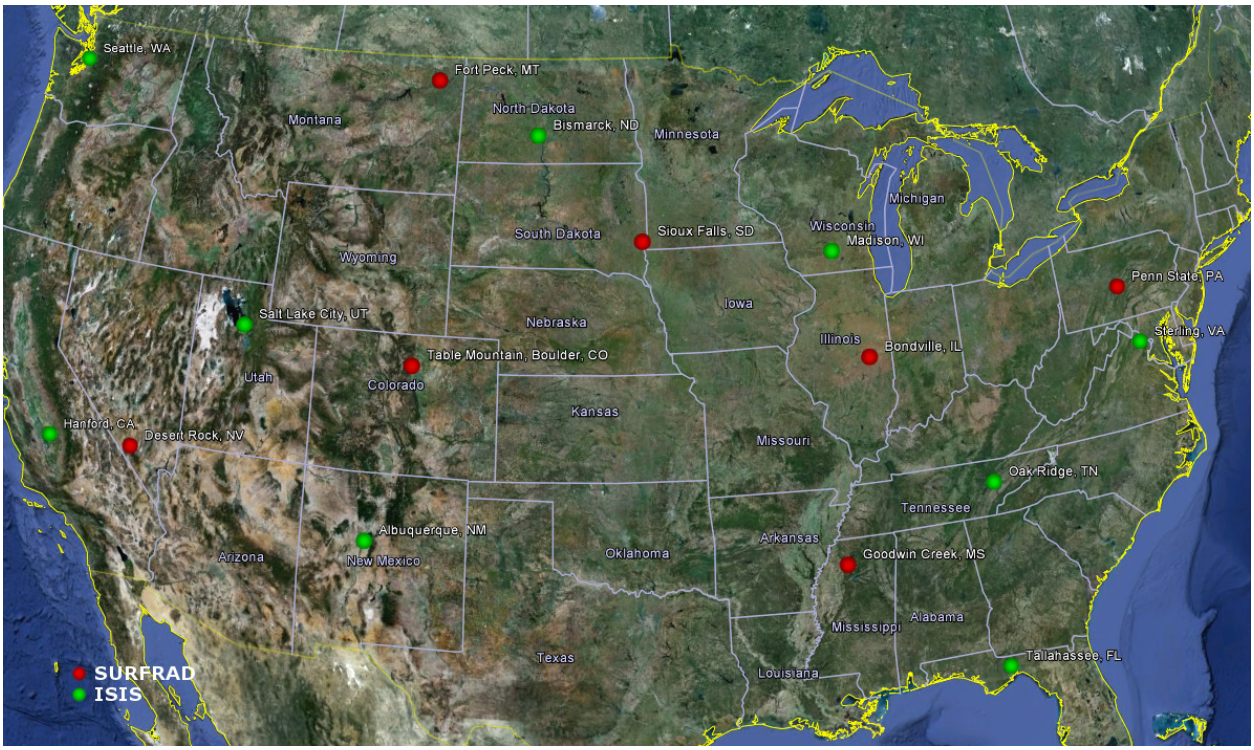

Figure 3.2. Location of ISIS and SURFRAD radiation monitors.

Rainfall amounts are estimated by the Parameter-elevation Relationships on Independent Slopes Model (PRISM) model, which uses an elevation-based regression model to analyze precipitation. PRISM's horizontal resolution is approximately 2 to 4 km and is re-projected to the WRF modeling domain for direct qualitative comparison to model estimates. The rainfall analysis is limited to the contiguous United States as the model utilizes elevation and measured precipitation data at automated weather stations.

Model performance (i.e., temperature, wind speed, and mixing ratio) is described using quantitative metrics: mean bias, mean (gross) error, fractional bias, and fractional error (Boylan and Russell, 2006). These metrics are useful because they describe model performance in the measured units of the meteorological variable and as a normalized percentage. Since wind direction is reported in compass degrees, estimating performance metrics for wind direction is problematic as modeled and observed northerly winds may be similar but differences would result in a very large artificial bias. For example, the absolute difference in a northerly wind direction measured in compass degrees of 1° and 359° is 358° when the actual difference is only 2°. To address this issue, wind field displacement, or the difference in the U and V vectors between modeled (M) and observed (O) values, is used to assess wind vector performance (Equation 1). Performance is best when these metrics approach 0.

(1) Wind displacement (km) = $(\mathbf{U}_M - \mathbf{U}_O + \mathbf{V}_M - \mathbf{V}_O)$*(1 km/1000 m)*(3600 s/hr)*(1 hr)

Rainfall performance is examined spatially using side-by-side comparisons of monthly total rainfall plots. The WRF model outputs predictions approximately 15 meters above the surface while observations are at 10 meters. WRF generates output at near instantaneous values (90 second time step) as opposed to longer averaging times taken at monitor stations. This should be considered when interpreting model performance metrics.

3.1 Model Performance for Winds

WRF-predicted wind speed estimates are compared to surface-based measurements made in the ds472 network described earlier. The results for the 36US (Figure 3.1.1) and 12US2 (Figure 3.1.2) domains are shown below.

At 36km, wind speeds are generally overpredicted across most hours of the day for all seasons, in terms of mean bias. In general, performance improves at 12km, with less overprediction. However, at 12km WRF tends to slightly overpredict wind speeds in the early morning and afternoon hours, while slightly underpredicting wind speeds in the late evening and overnight hours. There is no significant seasonal variability at either resolution in terms of wind speed.

The monthly spatial distributions of the wind speed biases (m/s) for all hours (Figures 3.1.3-3.1.6) and daytime hours[2] (Figures 3.1.7-3.1.10) are also presented. No appreciable difference is observed in the biases for daytime hours versus all hours. However, WRF tends to slightly overpredict wind speeds for areas in the eastern US and underpredicts wind speeds in the western US, particularly southern California. As noted above, these biases persist regardless of changes in season.

[2] 1200 GMT to 0000 GMT

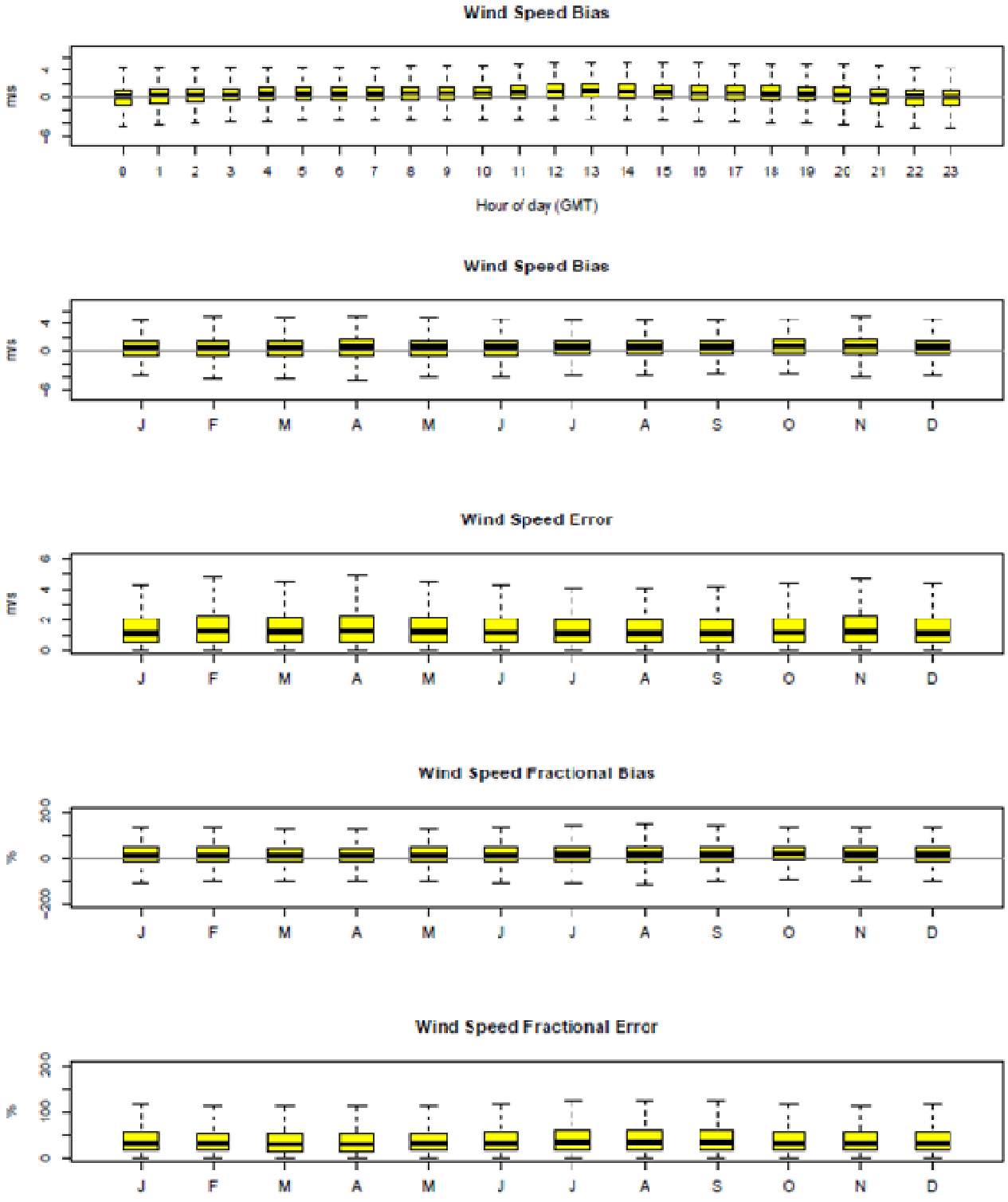

Figure 3.1.1. Distribution of hourly bias by hour and hourly bias, error, fractional bias, and fractional error for wind speed by month for 36US domain.

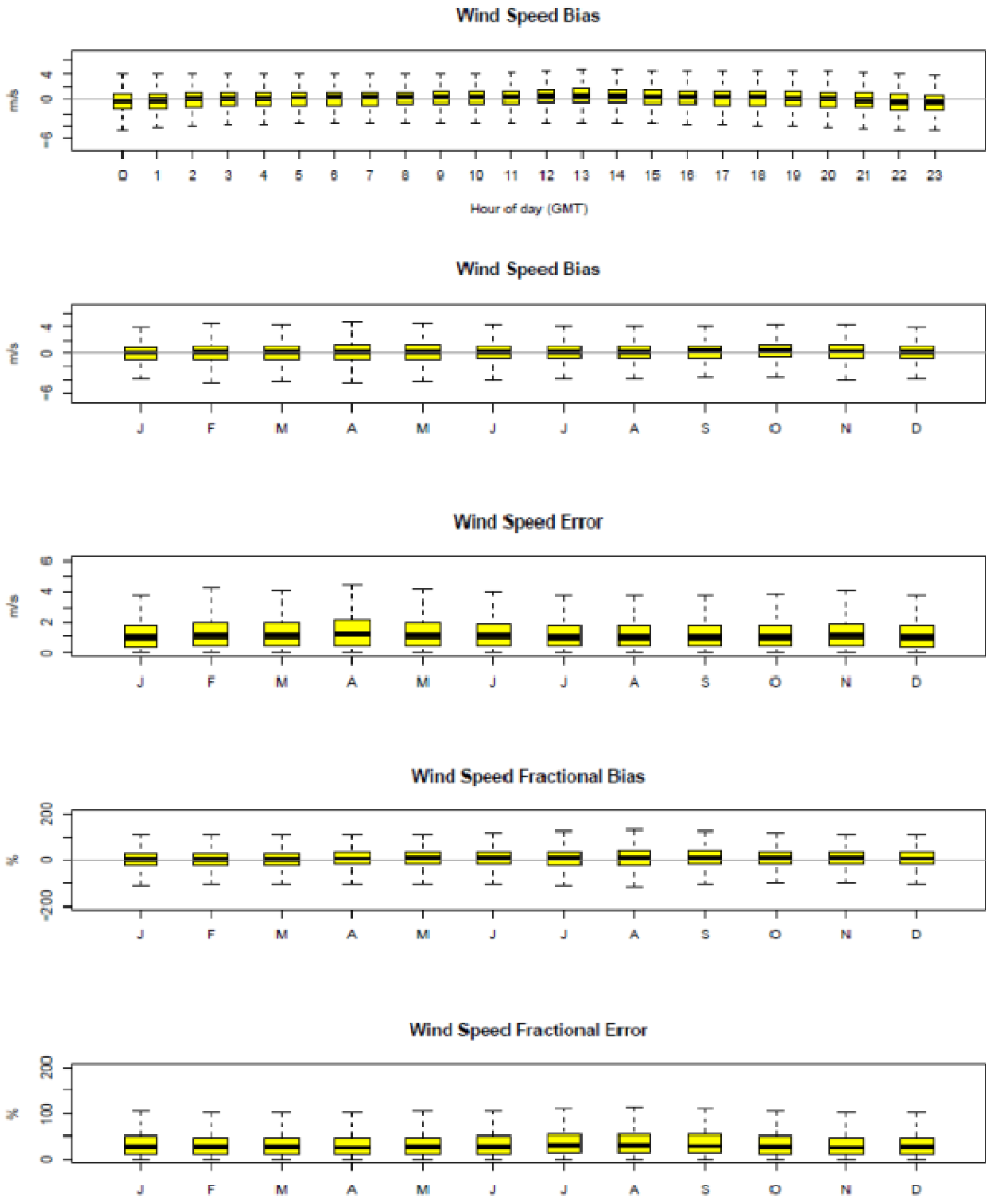

Figure 3.1.2. Distribution of hourly bias by hour and hourly bias, error, fractional bias, and fractional error for wind speed by month for 12US2 domain.

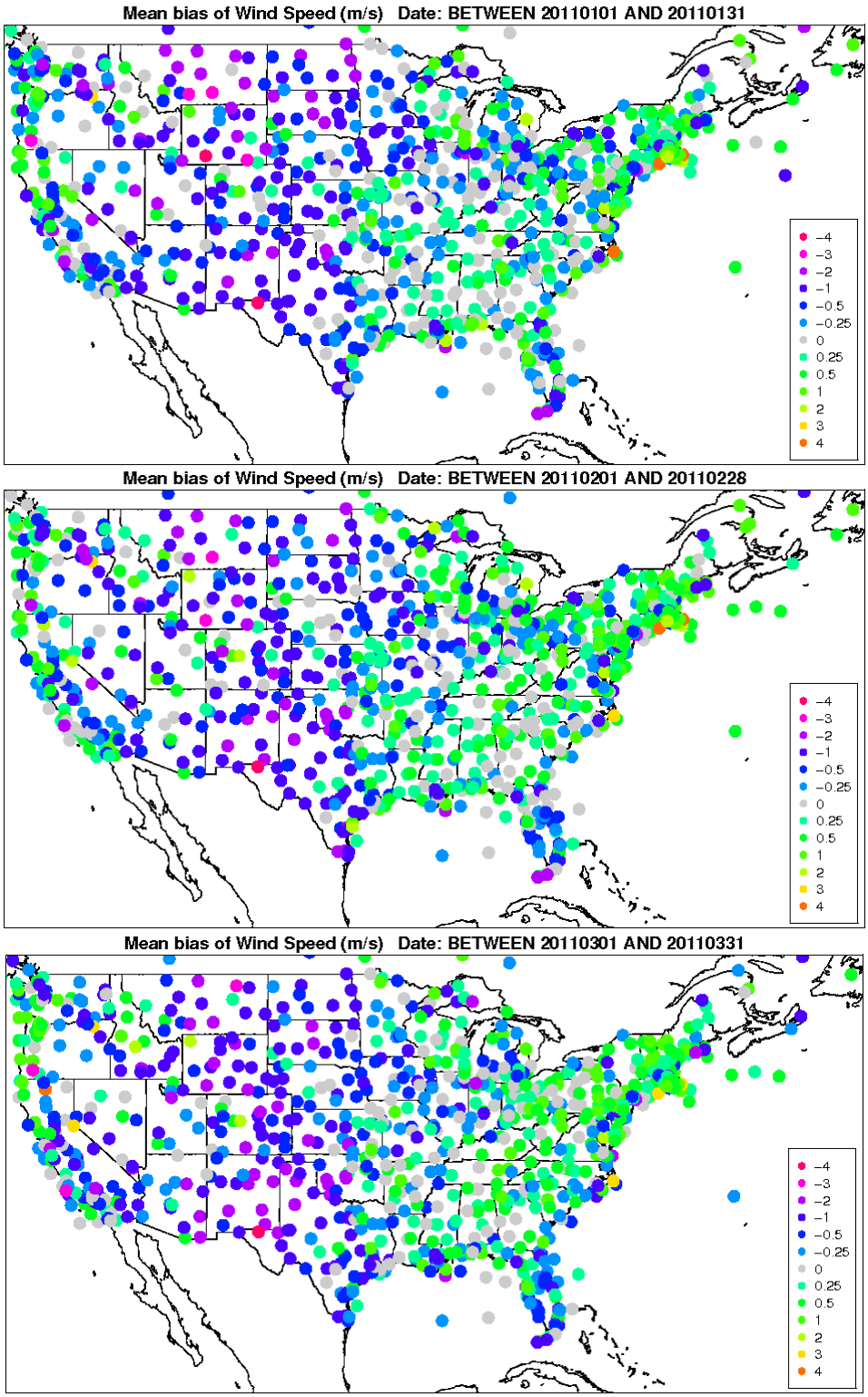

Figure 3.1.3. Spatial distribution of wind speed bias (m/s) across all hours for the months of January, February, and March (top to bottom) for the 12US2 domain.

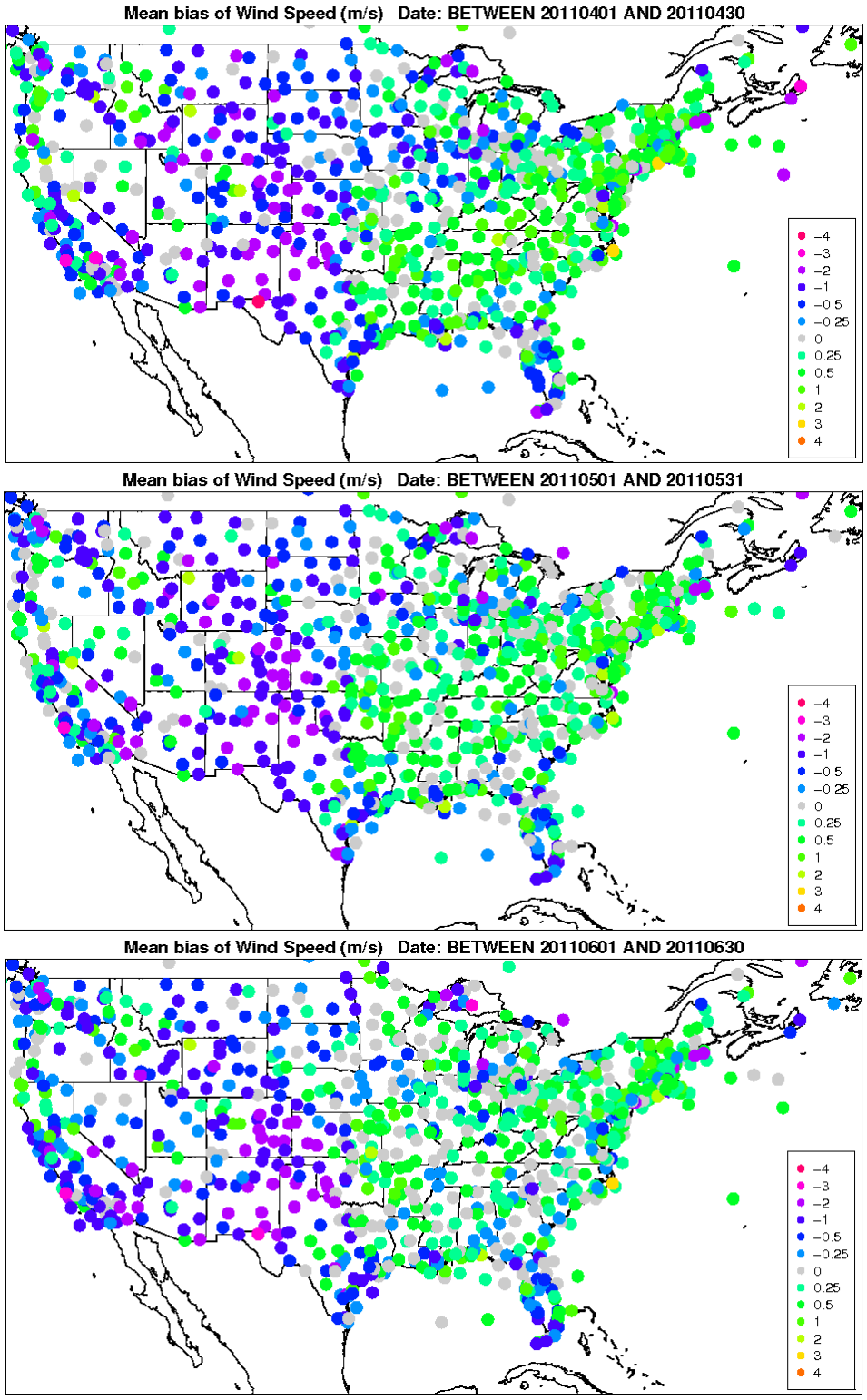

Figure 3.1.4. Spatial distribution of wind speed bias (m/s) across all hours for the months of April, May, and June (top to bottom) for the 12US2 domain.

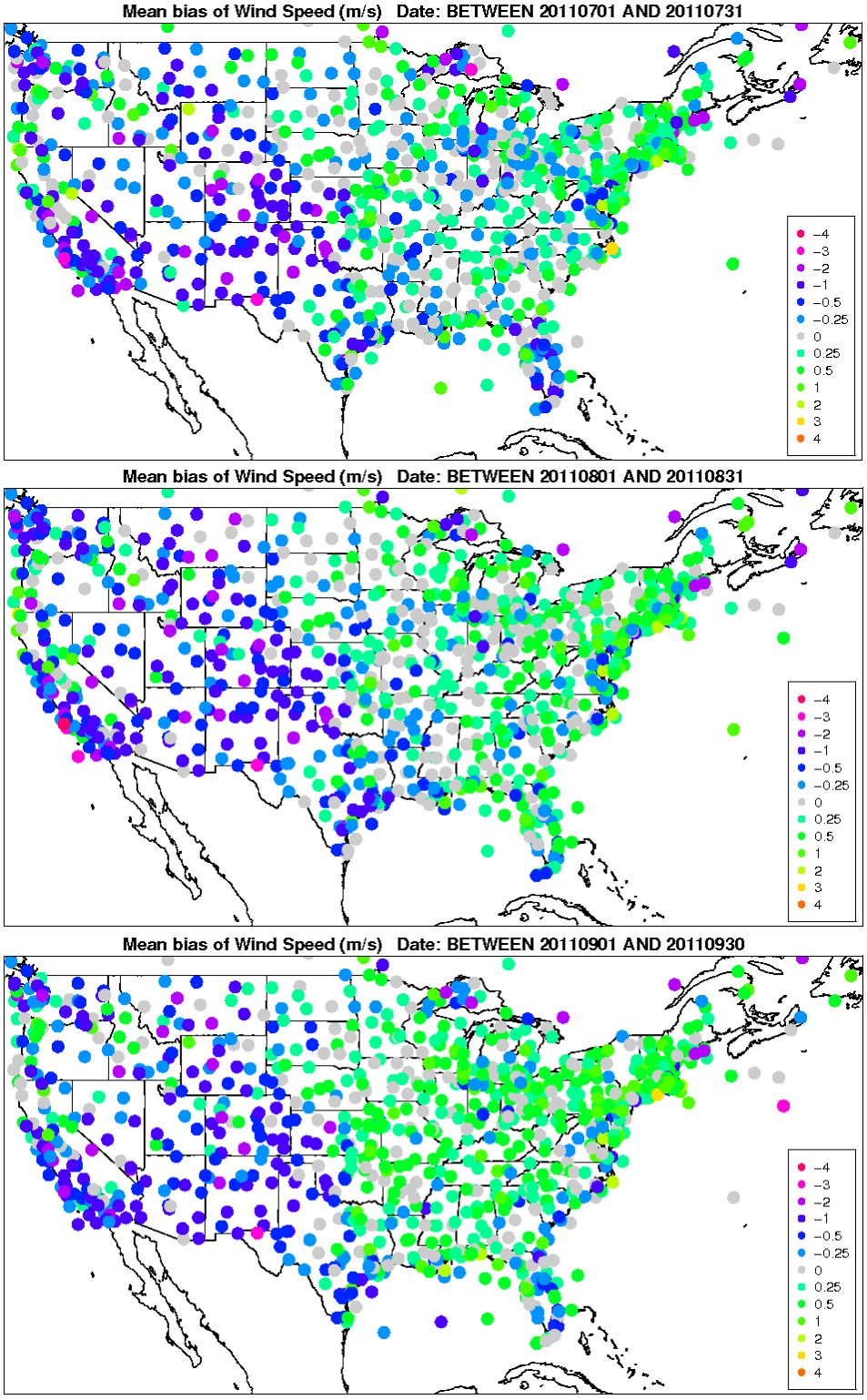

Figure 3.1.5. Spatial distribution of wind speed bias (m/s) across all hours for the months of July, August, and September (top to bottom) for the 12US2 domain.

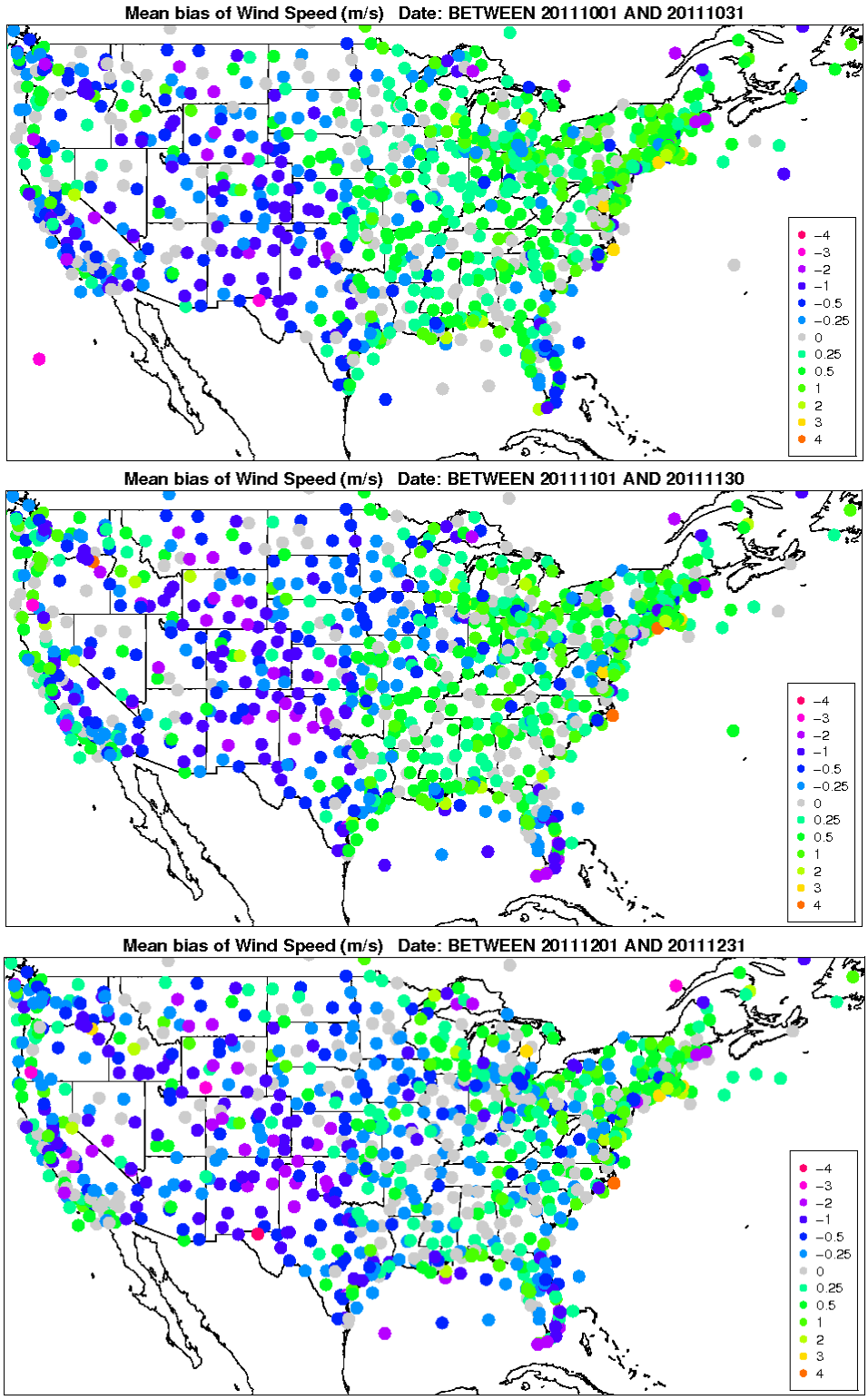

Figure 3.1.6. Spatial distribution of wind speed bias (m/s) across all hours for the months of October, November, and December (top to bottom) for the 12US2 domain.

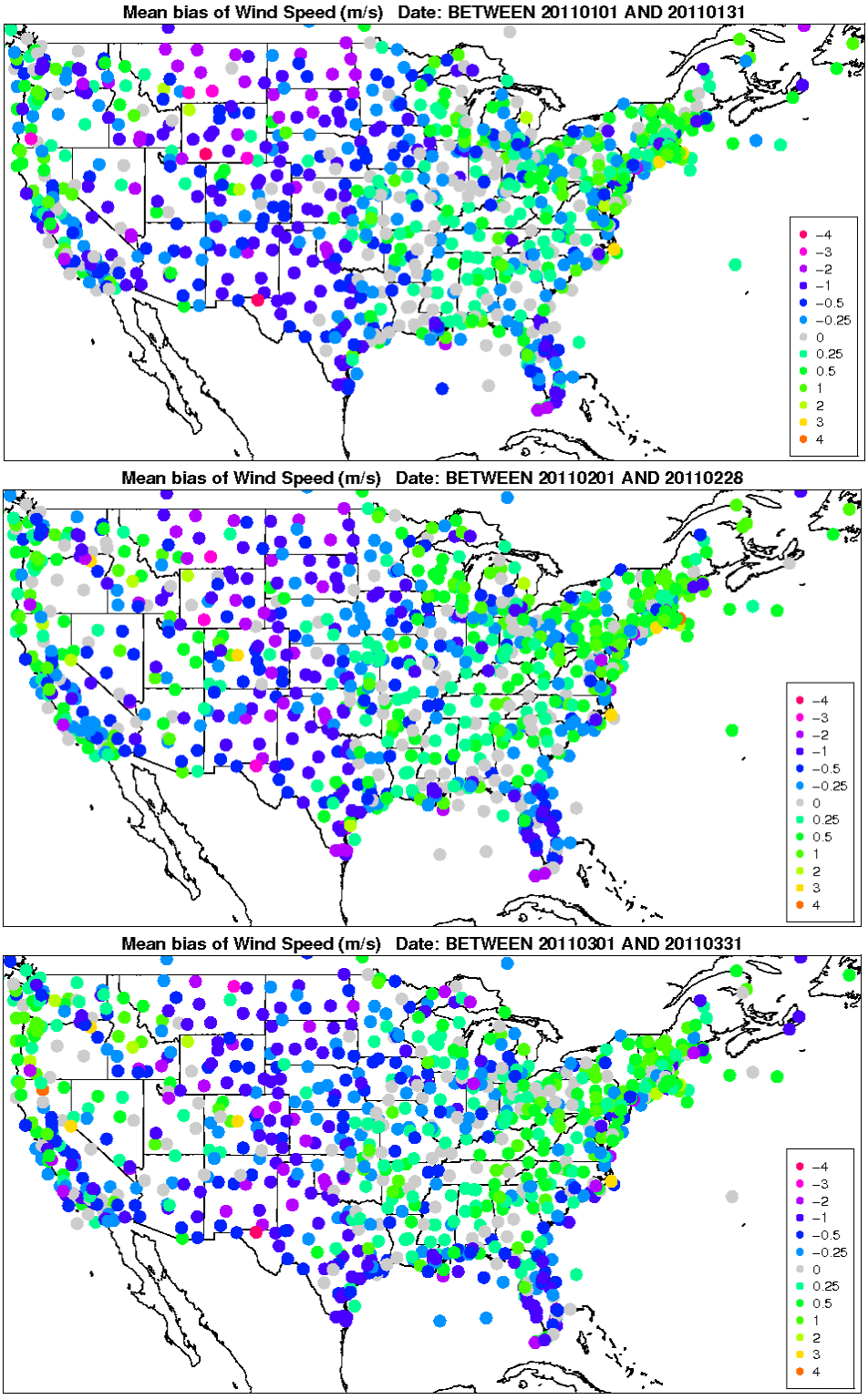

Figure 3.1.7. Spatial distribution of wind speed bias (m/s) across daytime hours for the months of January, February, and March (top to bottom) for the 12US2 domain.

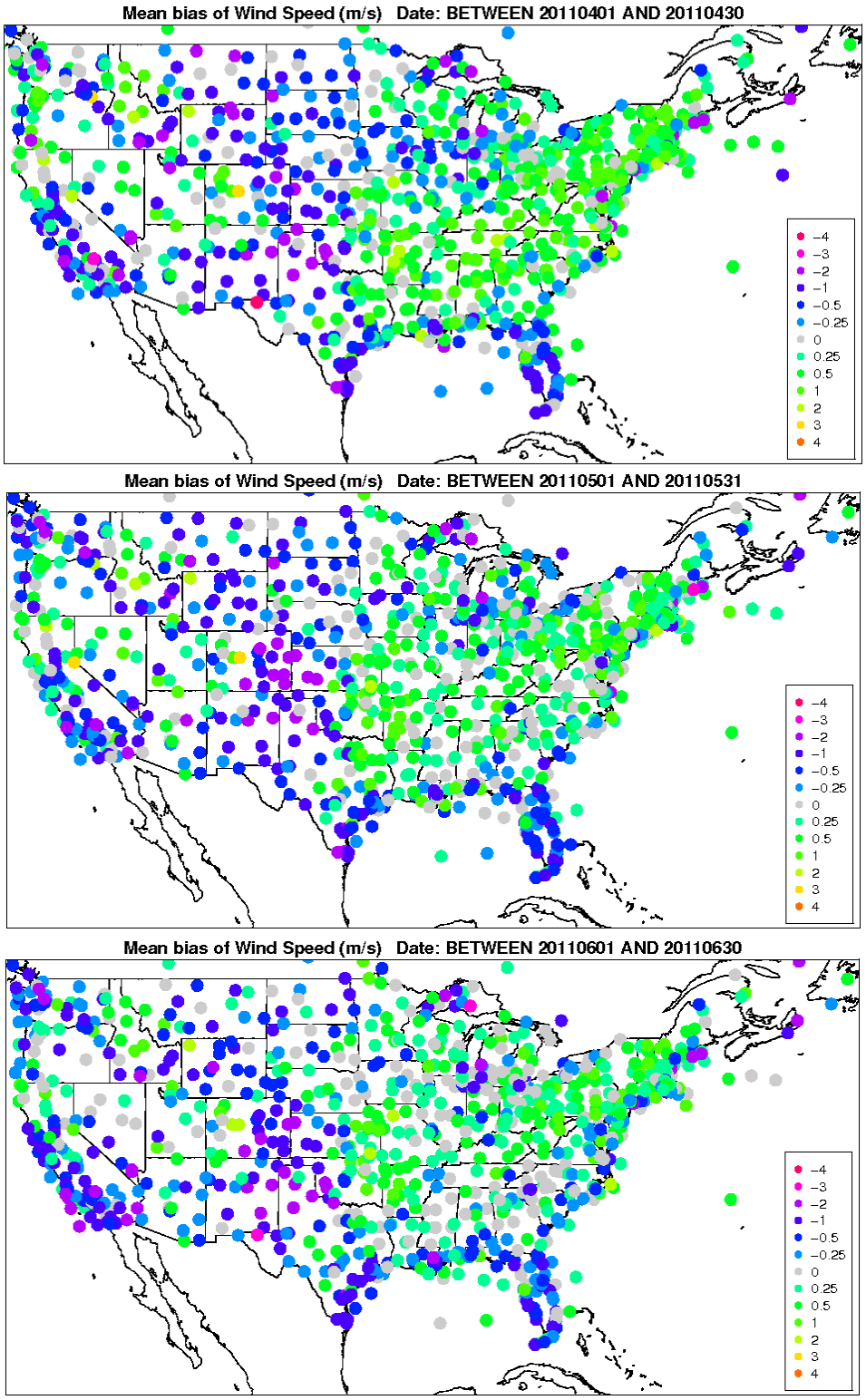

Figure 3.1.8. Spatial distribution of wind speed bias (m/s) across daytime hours for the months of April, May, and June (top to bottom) for the 12US2 domain.

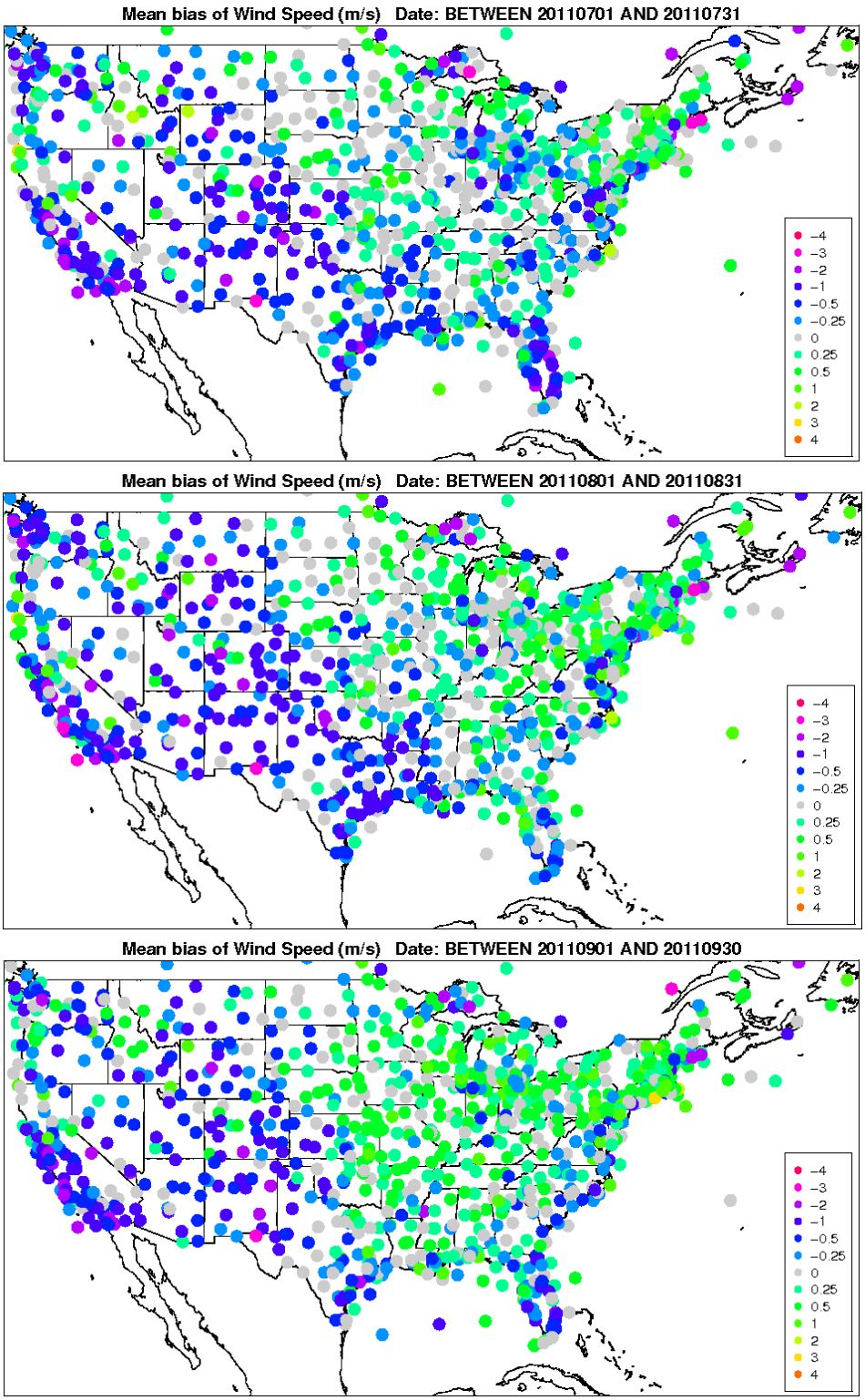

Figure 3.1.9. Spatial distribution of wind speed bias (m/s) across daytime hours for the months of July, August, and September (top to bottom) for the 12US2 domain.

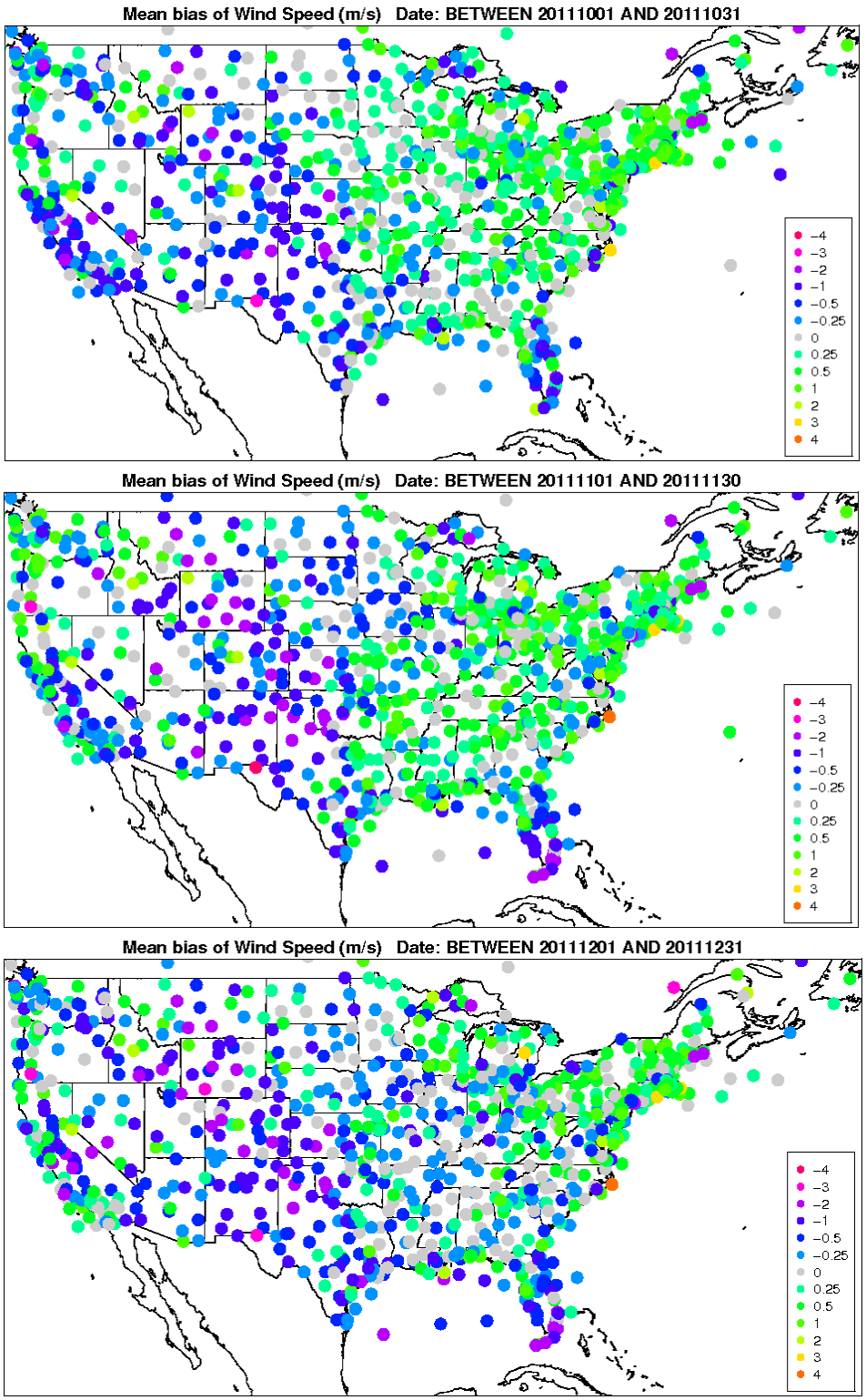

Figure 3.1.10. Spatial distribution of wind speed bias (m/s) across daytime hours for the months of October, November, and December (top to bottom) for the 12US2 domain.

Wind vector displacement (km) is presented below for the 36US (Figure 3.1.11) and 12US2 (Figure 3.1.12) domains utilizing the ds472 observation network described earlier. These plots show the entire distribution of hourly wind displacement by month and by hour of the day. Overall, model performance is adequate in terms of wind vector differences. Both the 36- and 12-km simulations have a mean wind displacement of around 5km. Since this difference is less than the horizontal resolution, negligible impacts due to wind displacement are expected.

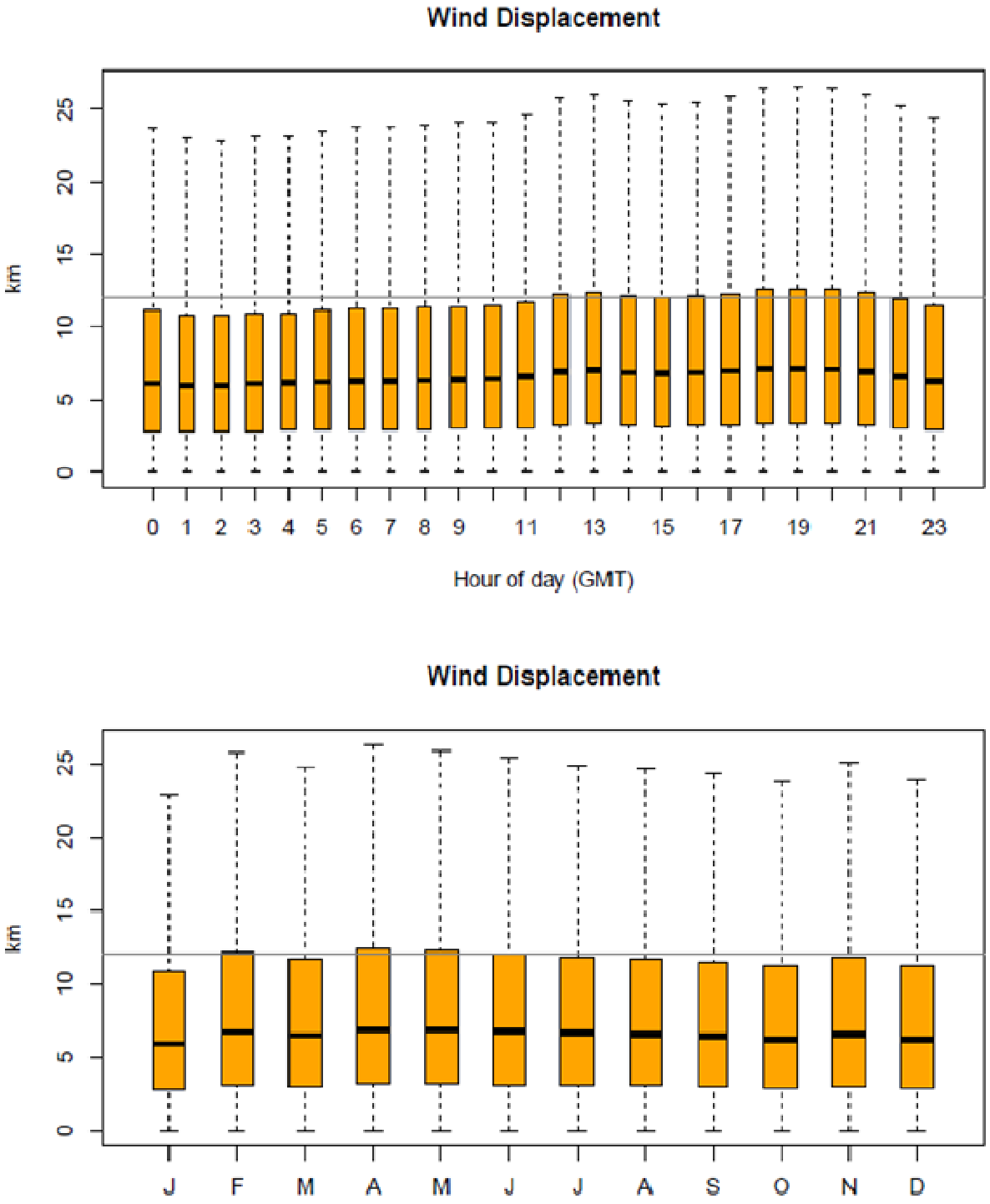

Figure 3.1.11. Distribution of hourly wind displacement (km) by hour and month for the 36US domain.

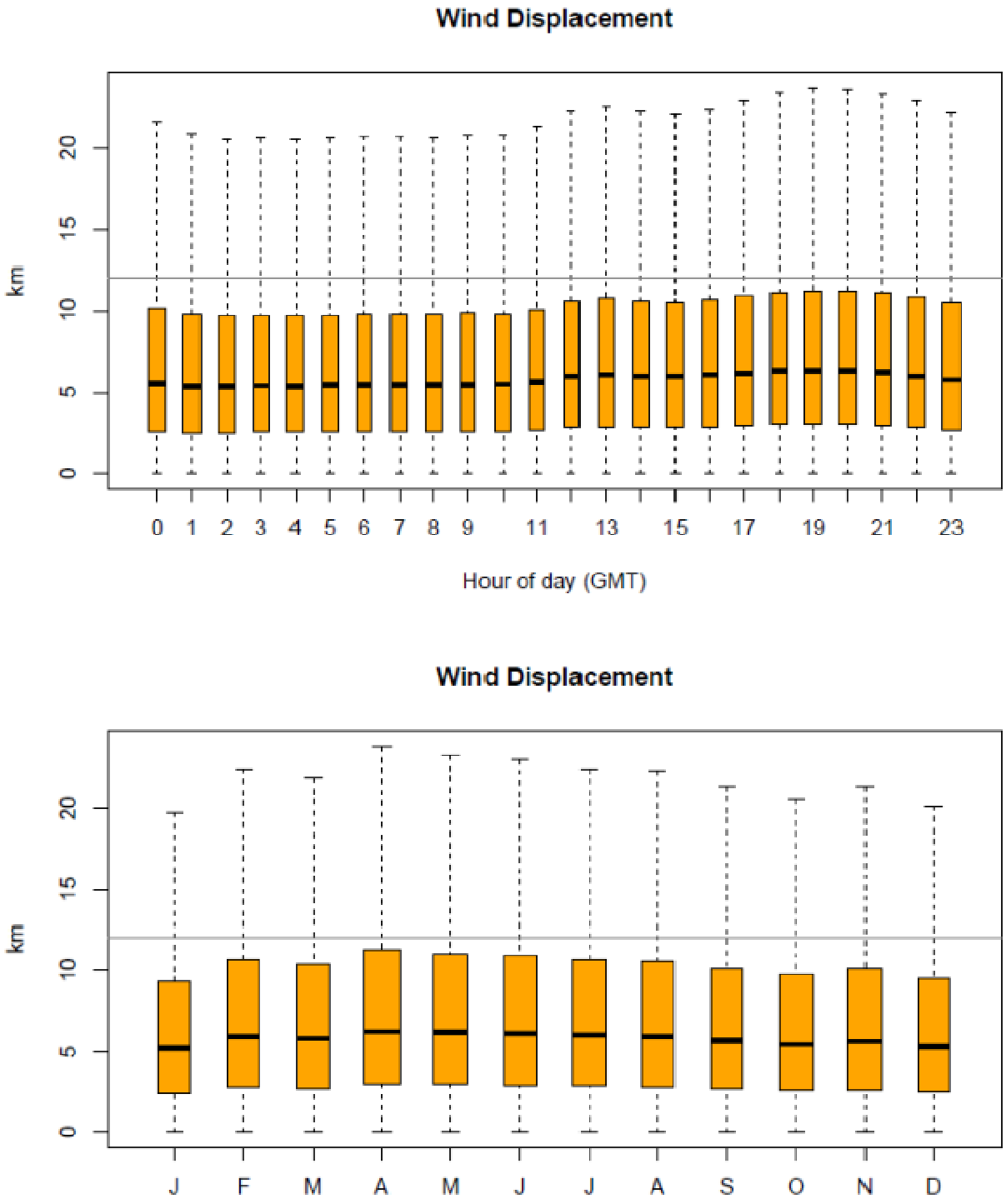

Figure 3.1.12. Distribution of hourly wind displacement (km) by hour and month for the 12US2 domain.

3.2 Temperature

Temperature estimates are compared to the ds472 observation network described earlier and are presented below for the 36US (Figure 3.2.1) and 12US2 (Figure 3.2.2) domains.

Overall, WRF slightly underpredicts surface temperature at both 36- and 12-km for most hours, with a slight overprediction in the early morning hours. In the summer months (June, July, and August), there appears to be less variability in both simulations, with the inner quartile range (IQR) more closely centered around zero in both simulations. Overall, with an average IQR of +/- 2 degrees Celsius (C), this is considered good model performance.

In Figures 3.2.3-3.2.6 and 3.2.7-3.2.10 the monthly spatial distributions of the temperature bias for the 12km simulation is presented for all hours and daytime only, respectively. Overall, a persistent slight underprediction of temperature is noted for most months. During daytime hours, a more significant underprediction of temperature is noted across much of the central and eastern US when compared to all hours. In areas of the western US, there is a persistent slight overprediction of temperature, regardless of season.

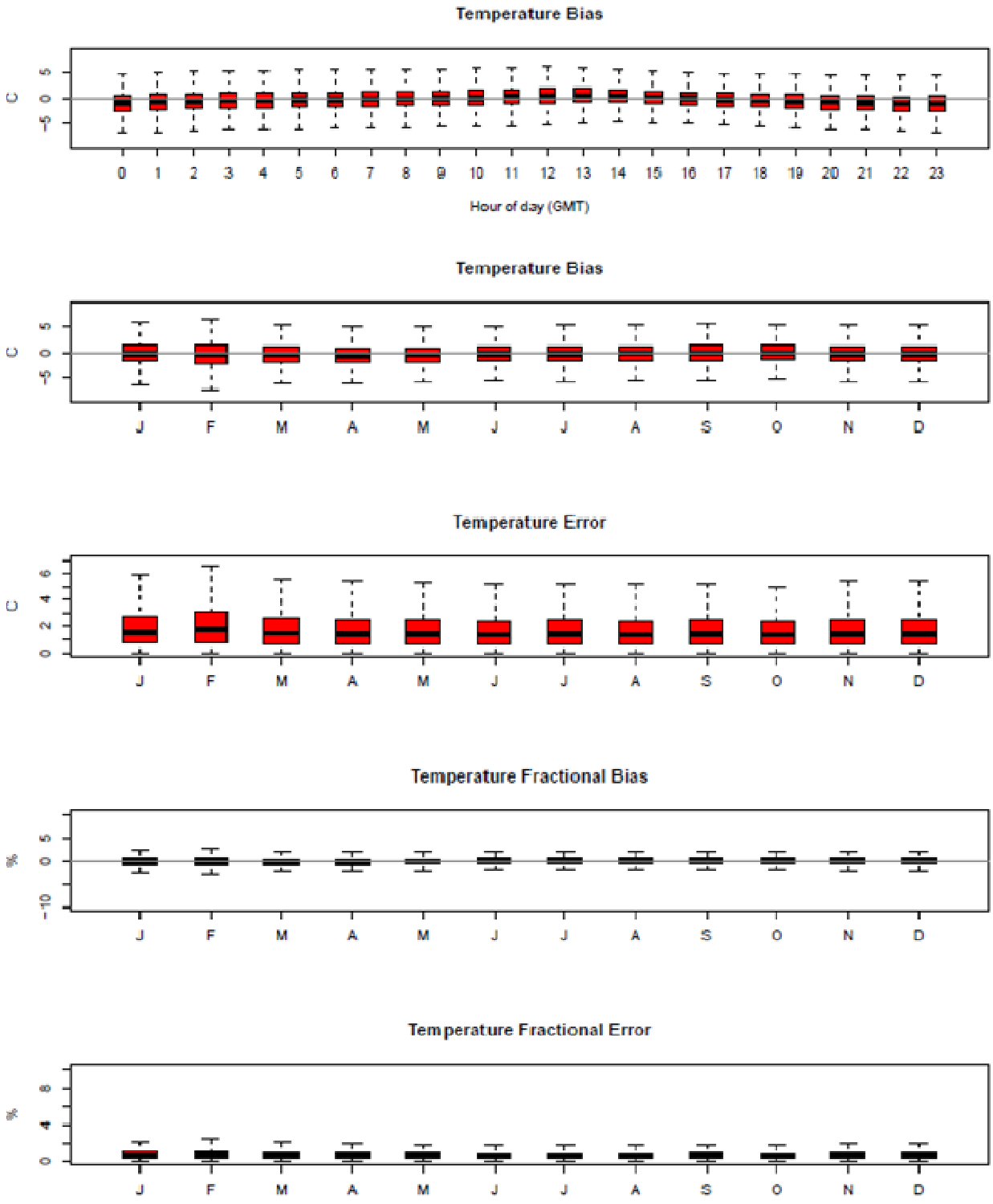

Figure 3.2.1. Distribution of hourly bias by hour and hourly bias, error, fractional bias, and fractional error for temperature by month for the 36US domain.

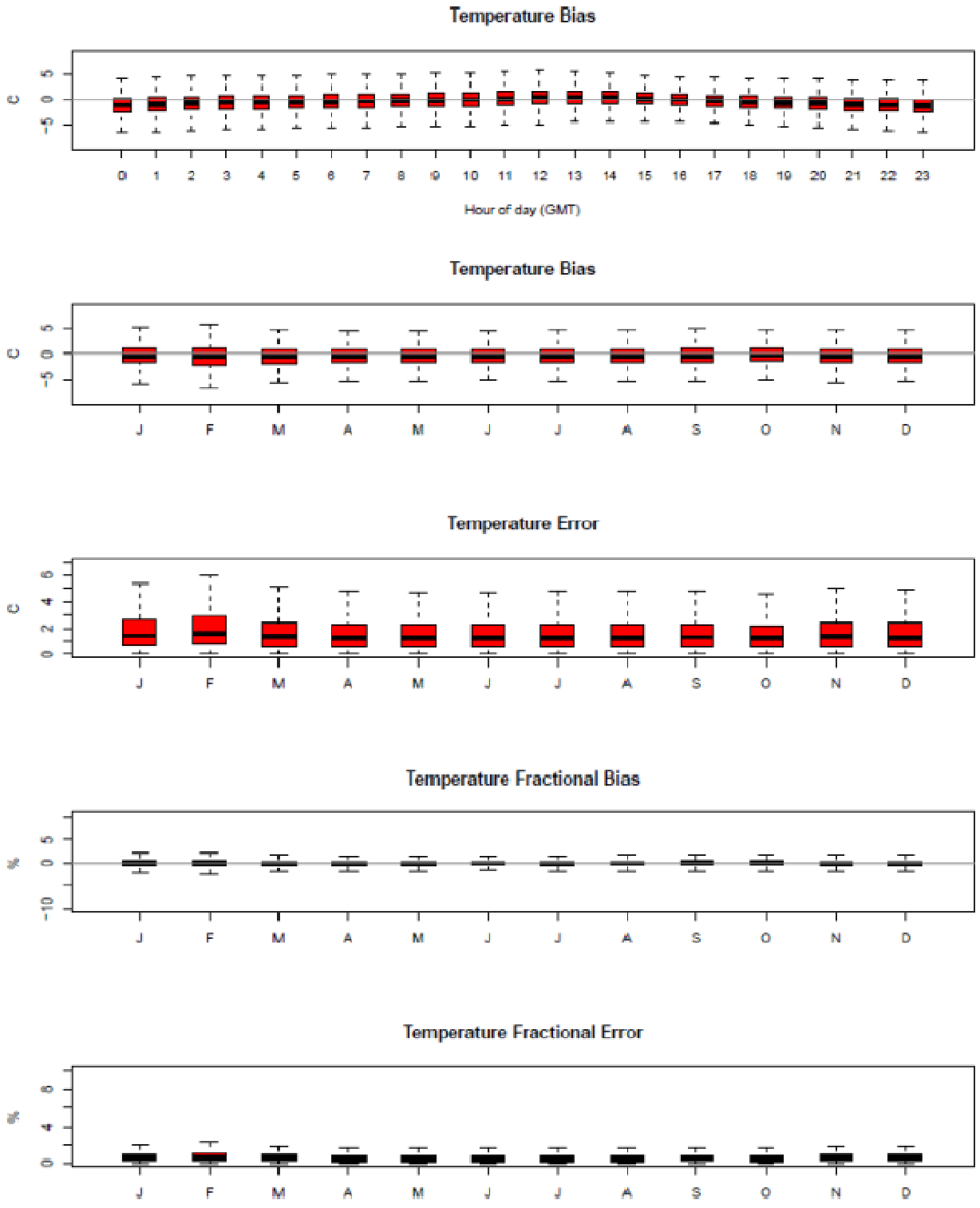

Figure 3.2.2. Distribution of hourly bias by hour and hourly bias, error, fractional bias, and fractional error for temperature by month for the 12US2 domain.

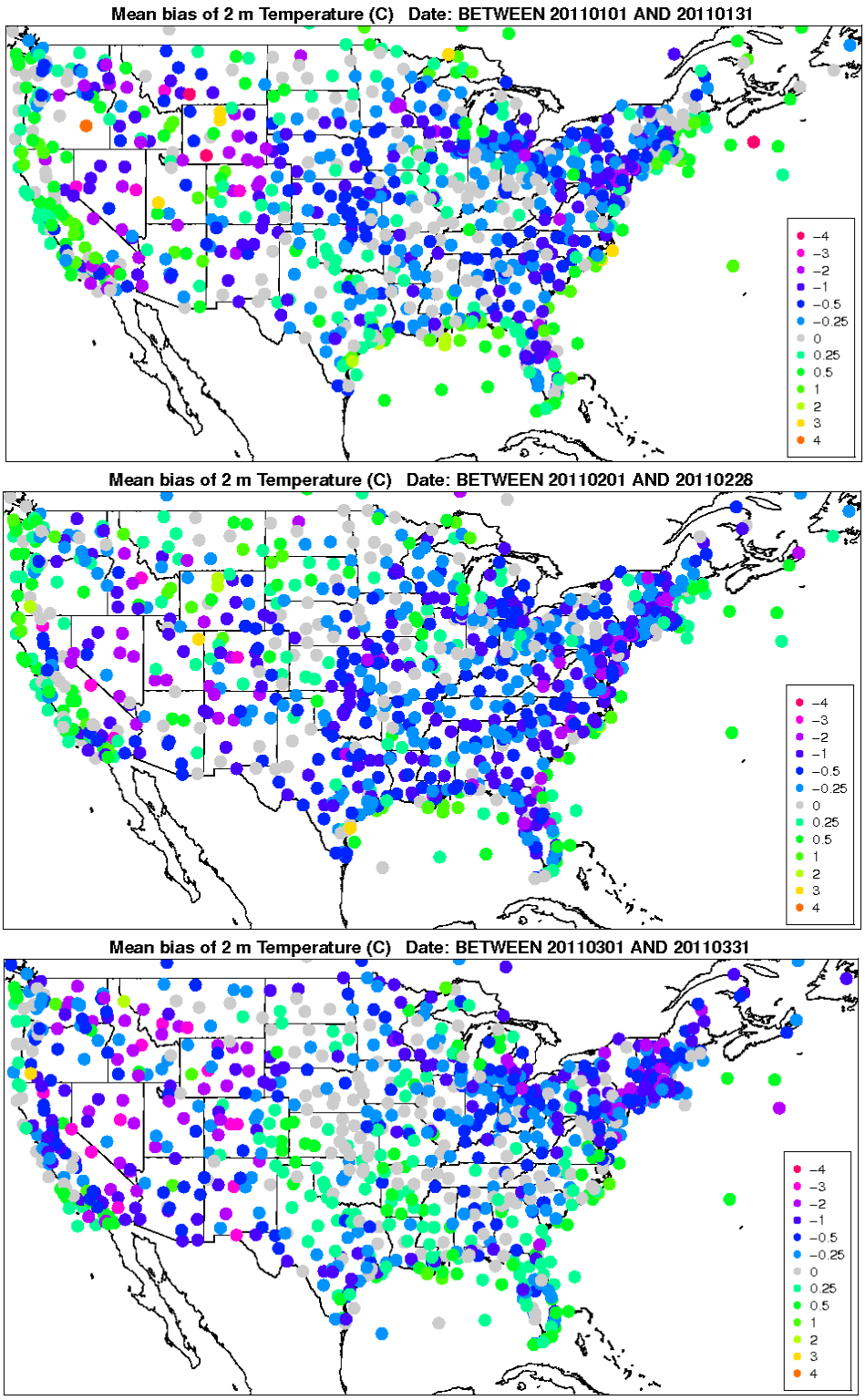

Figure 3.2.3. Spatial distribution of temperature bias (C) across all hours for the months of January, February, and March (top to bottom) for the 12US2 domain.

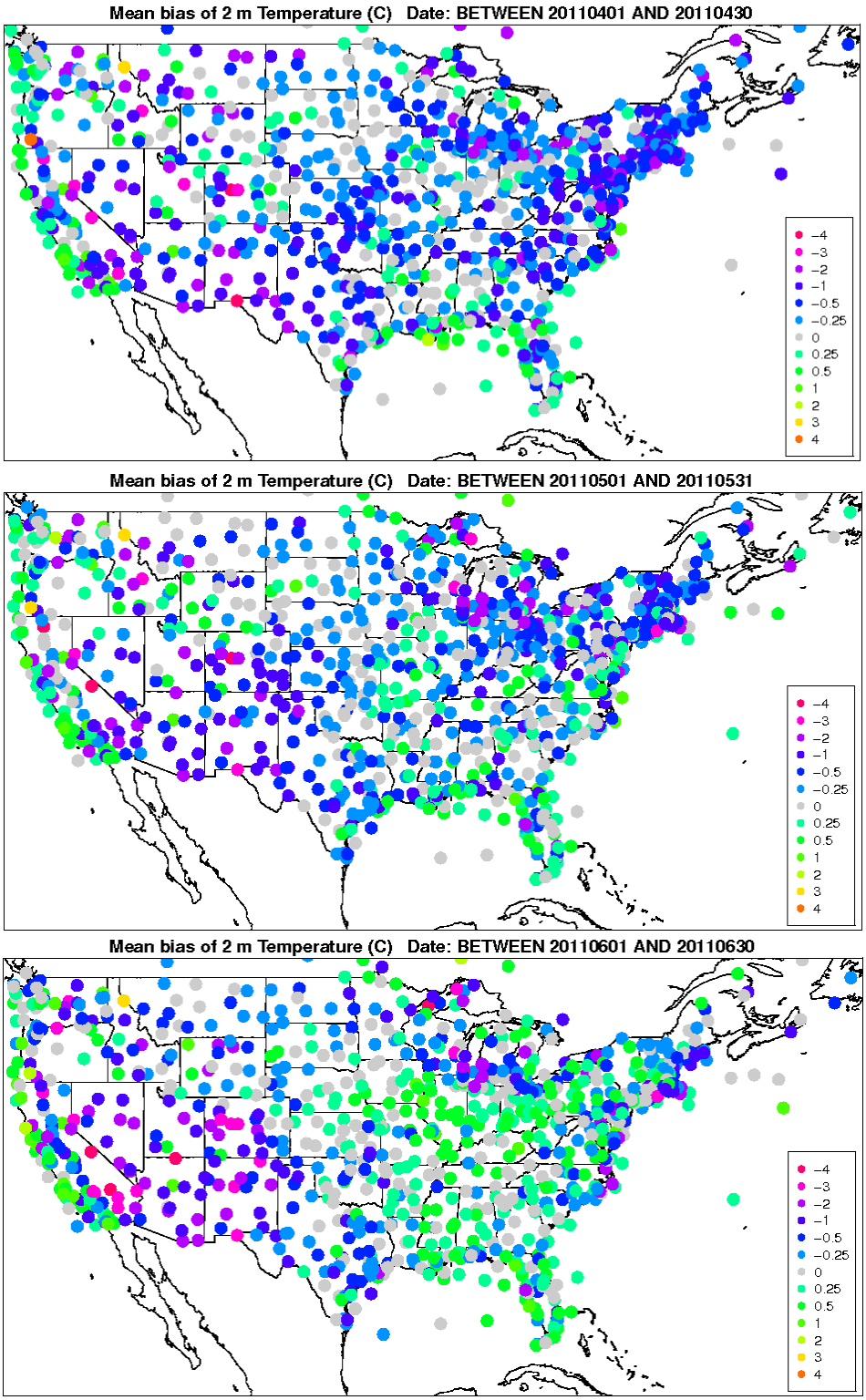

Figure 3.2.4. Spatial distribution of temperature bias (C) across all hours for the months of April, May, and June (top to bottom) for the 12US2 domain.

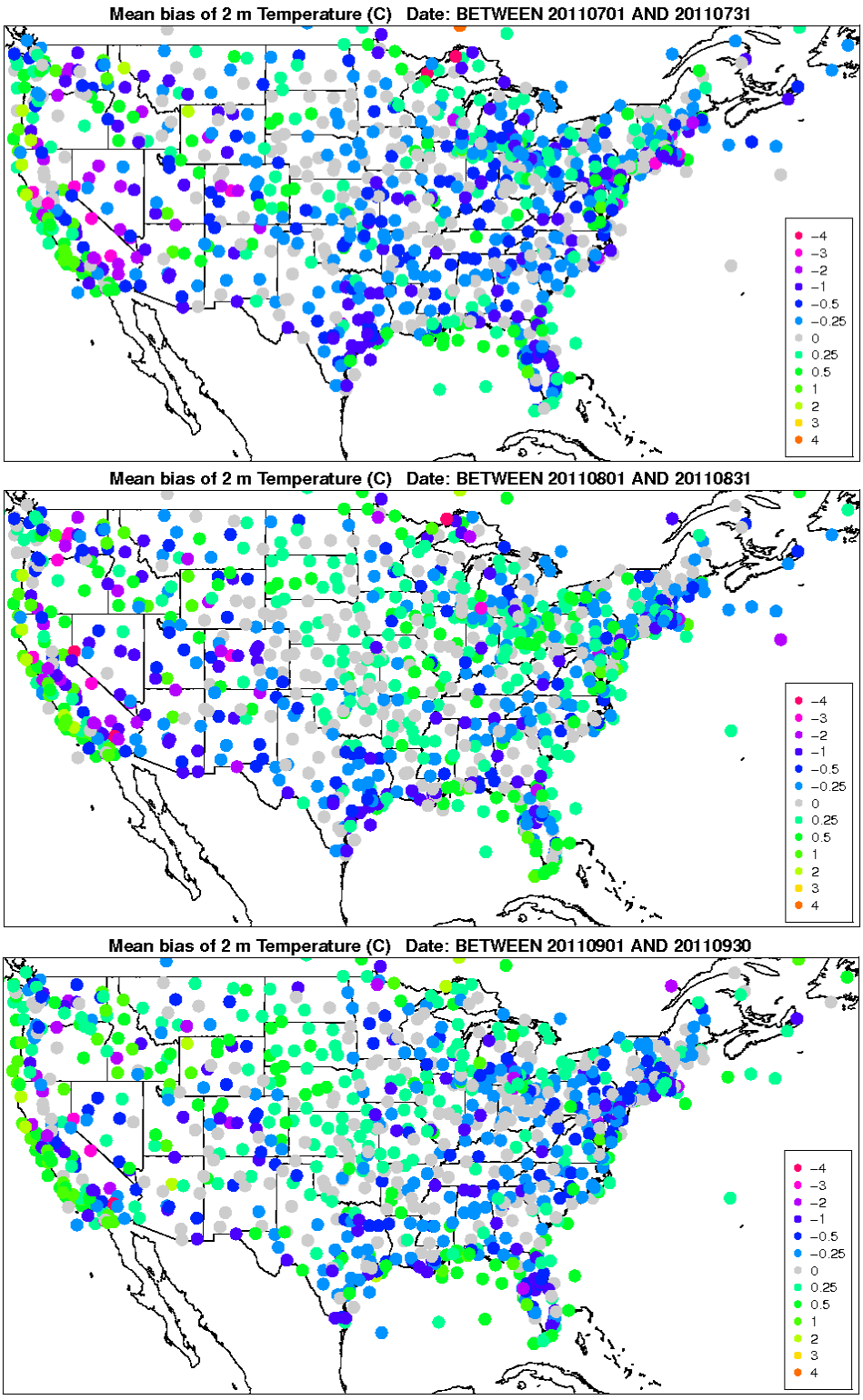

Figure 3.2.5. Spatial distribution of temperature bias (C) across all hours for the months of July, August, and September (top to bottom) for the 12US2 domain.

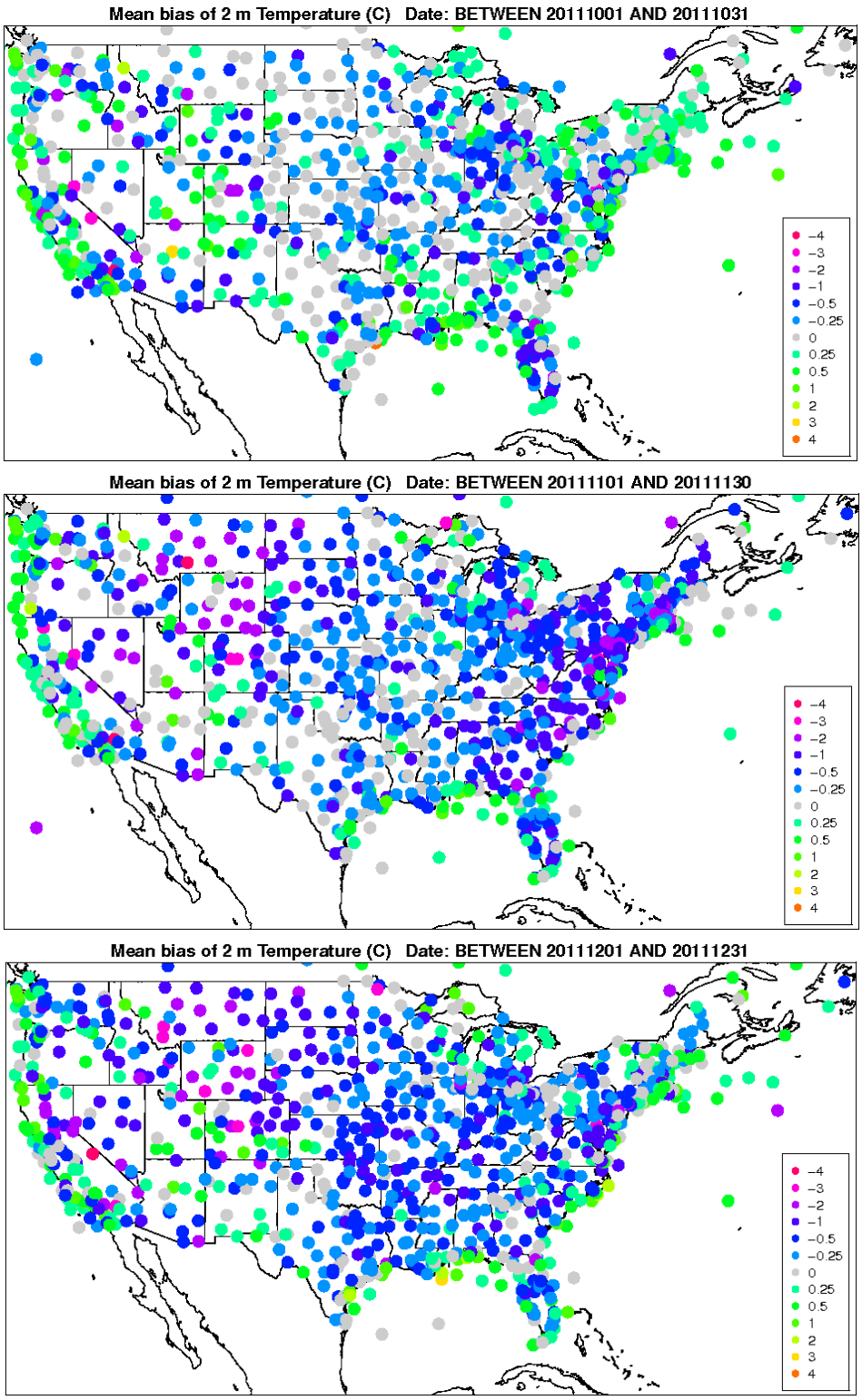

Figure 3.2.6. Spatial distribution of temperature bias (C) across all hours for the months of October, November, and December (top to bottom) for the 12US2 domain.

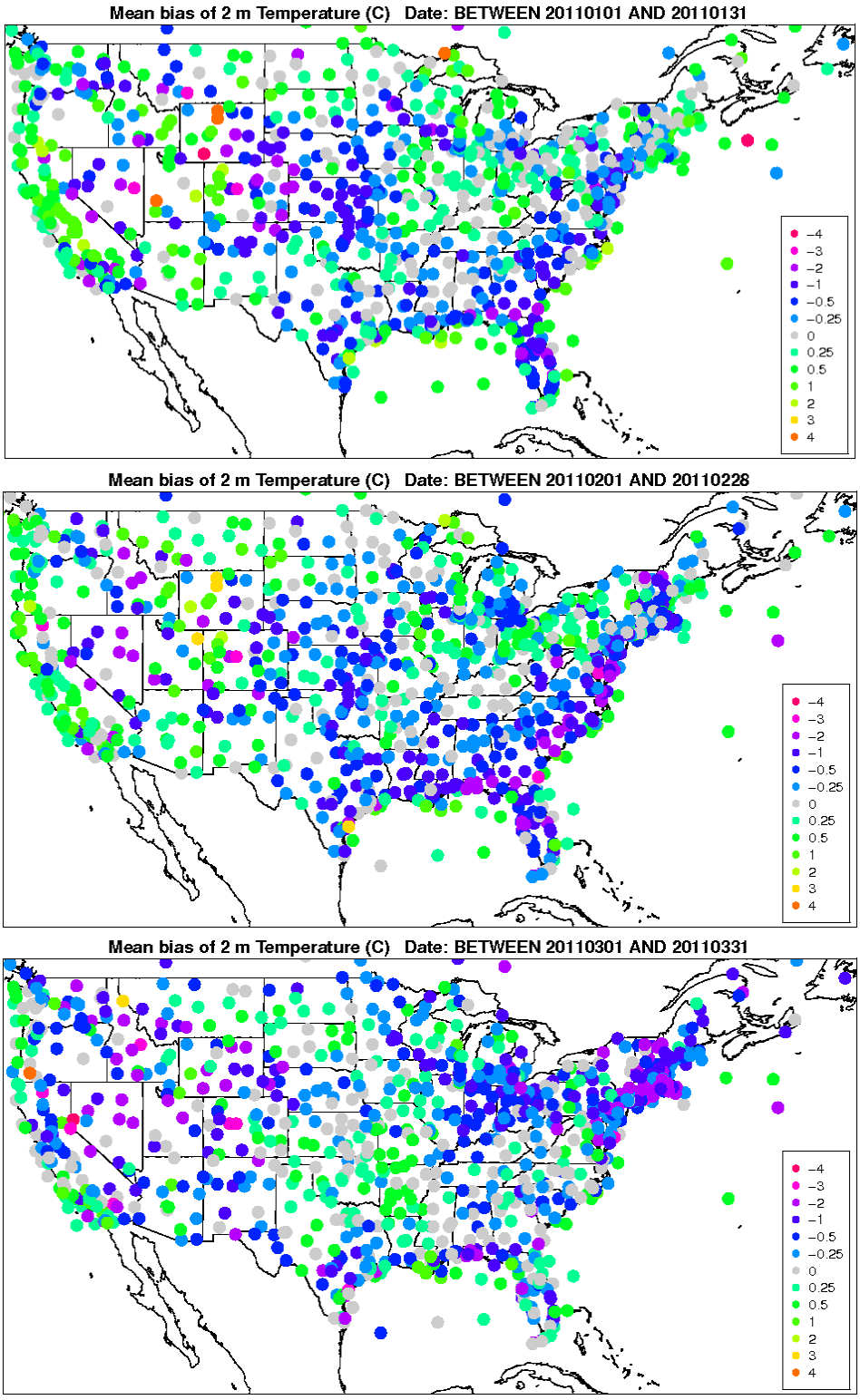

Figure 3.2.7. Spatial distribution of temperature bias (C) across daytime hours for the months of January, February, and March (top to bottom) for the 12US2 domain.

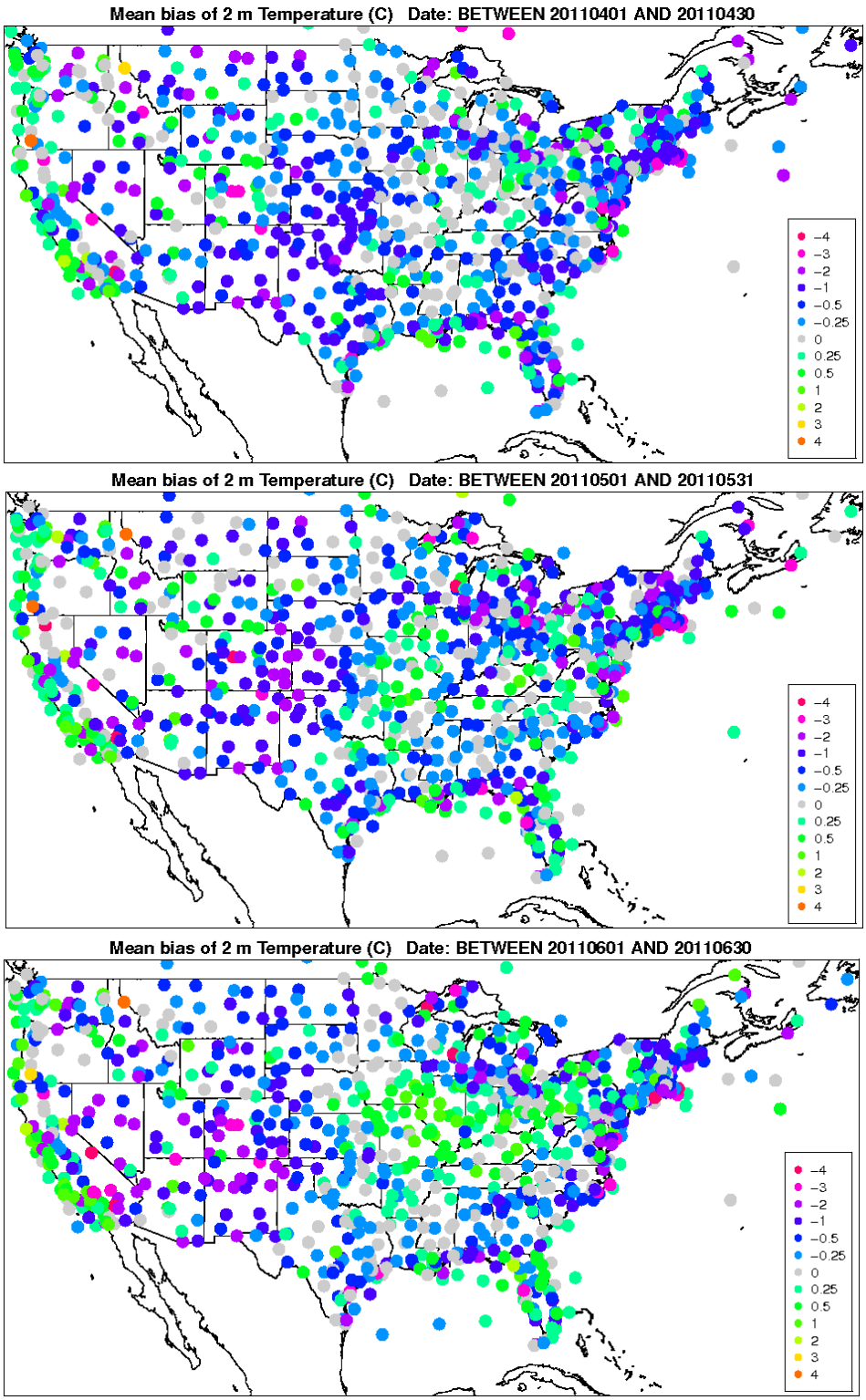

Figure 3.2.8. Spatial distribution of temperature bias (C) across daytime hours for the months of April, May, and June (top to bottom) for the 12US2 domain.

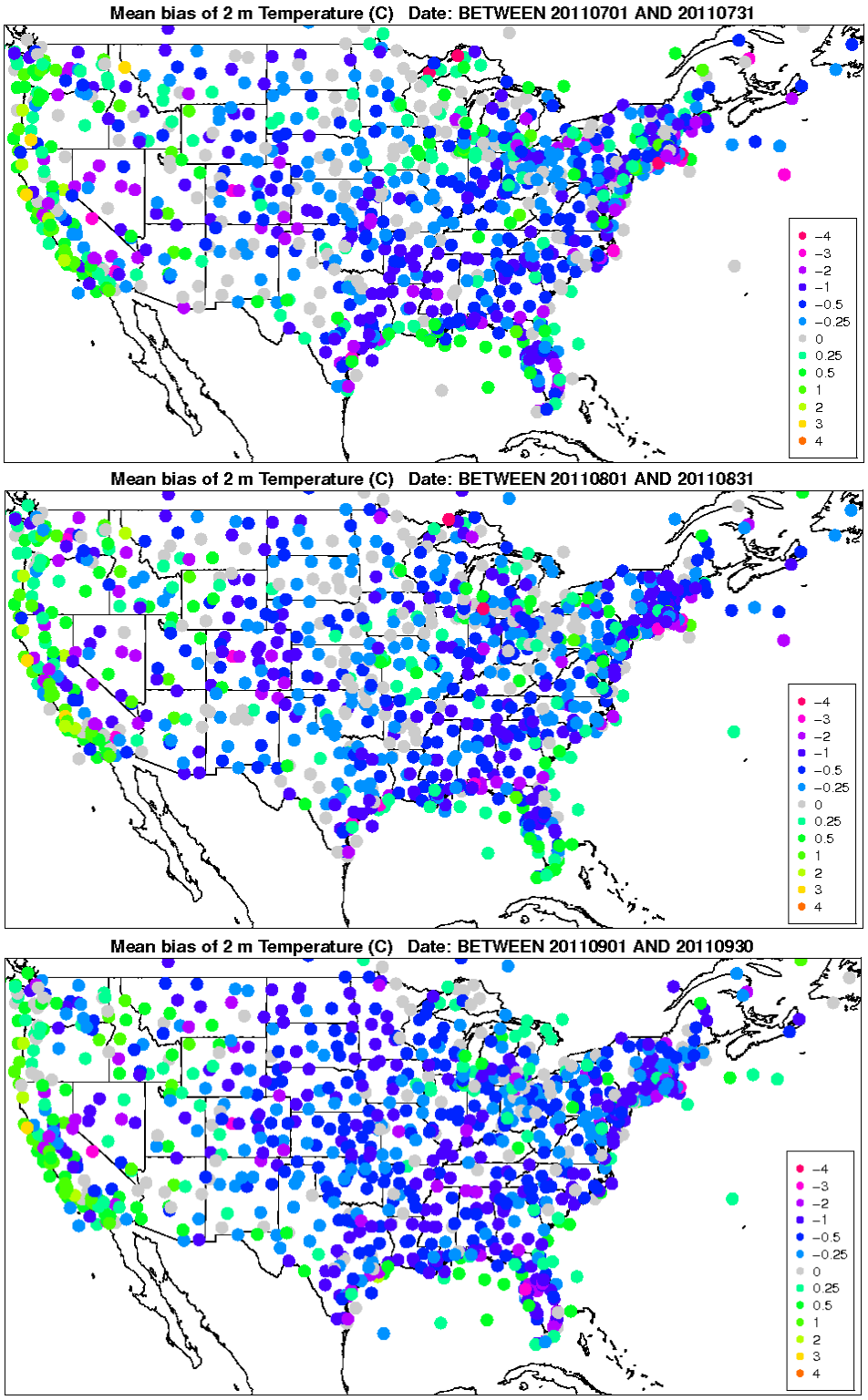

Figure 3.2.9. Spatial distribution of temperature bias (C) across daytime hours for the months of July, August, and September (top to bottom) for the 12US2 domain.

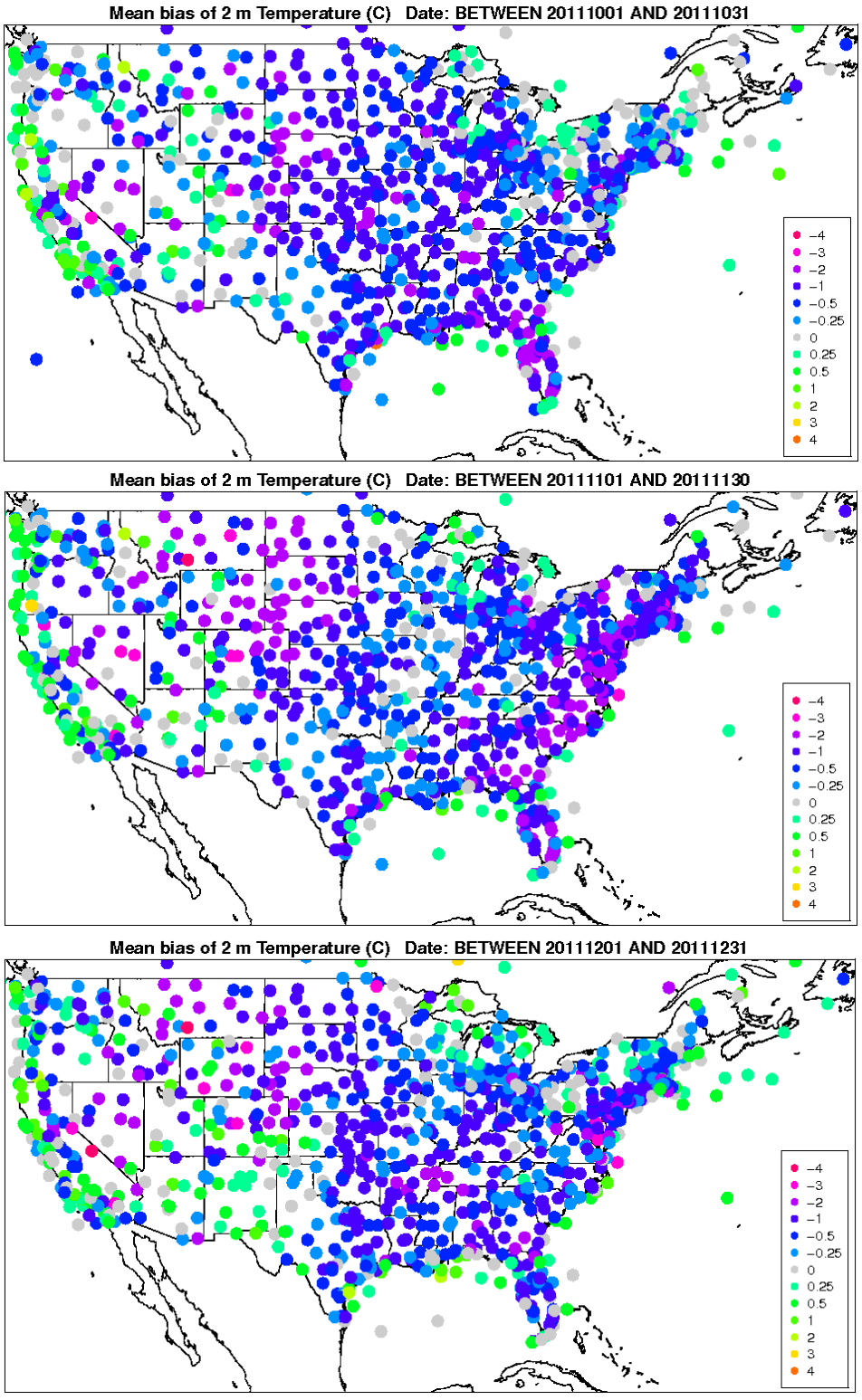

Figure 3.2.10. Spatial distribution of temperature bias (C) across daytime hours for the months of October, November, and December (top to bottom) for the 12US2 domain.

3.3 Mixing Ratio

Water mixing ratio estimates are compared to the ds472 observation network described earlier and are presented below for the 36US (Figure 3.3.1) and 12US2 (Figure 3.3.2) domains.

In either simulation, no significant positive or negative bias is observed. However, WRF tends to be slightly drier in the early afternoon hours relative to the rest of the day. Additionally, there is more uncertainty in model predictions during the spring and summer months. This increase in error is explained by the increased convective activity and influx of moist air masses that are typical of that time of year. In general, WRF performance was adequate for water vapor mixing ratio.

The monthly spatial distributions of the mixing ratio bias for the 12km simulation are shown in Figures 3.3.3-3.3.6 (all hours) and 3.3.7-3.3.10 (daytime). Little appreciable difference is observed in the biases either across all hours or just daytime. This is to be expected since water vapor mixing ratio has less temporal variability when compared to other variables (i.e., temperature). In the central and western US, mixing ratio is generally underpredicted across all months of the year, whereas a slight overprediction is observed in the eastern states for most months. In October and November, WRF exhibits a general underprediction for most locations across the country.

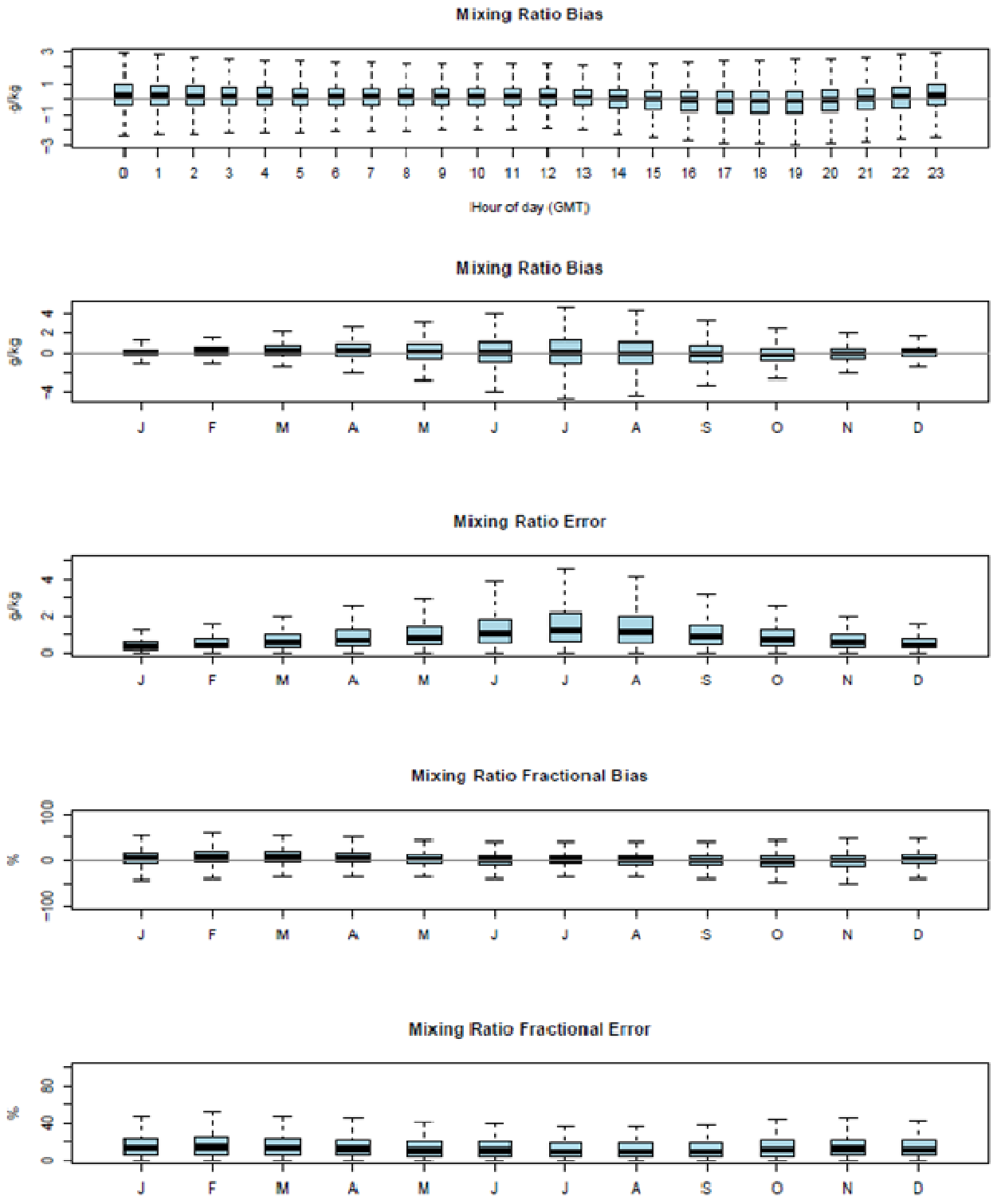

Figure 3.3.1. Distribution of hourly bias by hour and hourly bias, error, fractional bias, and fractional error for water vapor mixing ratio by month for the 36US domain.

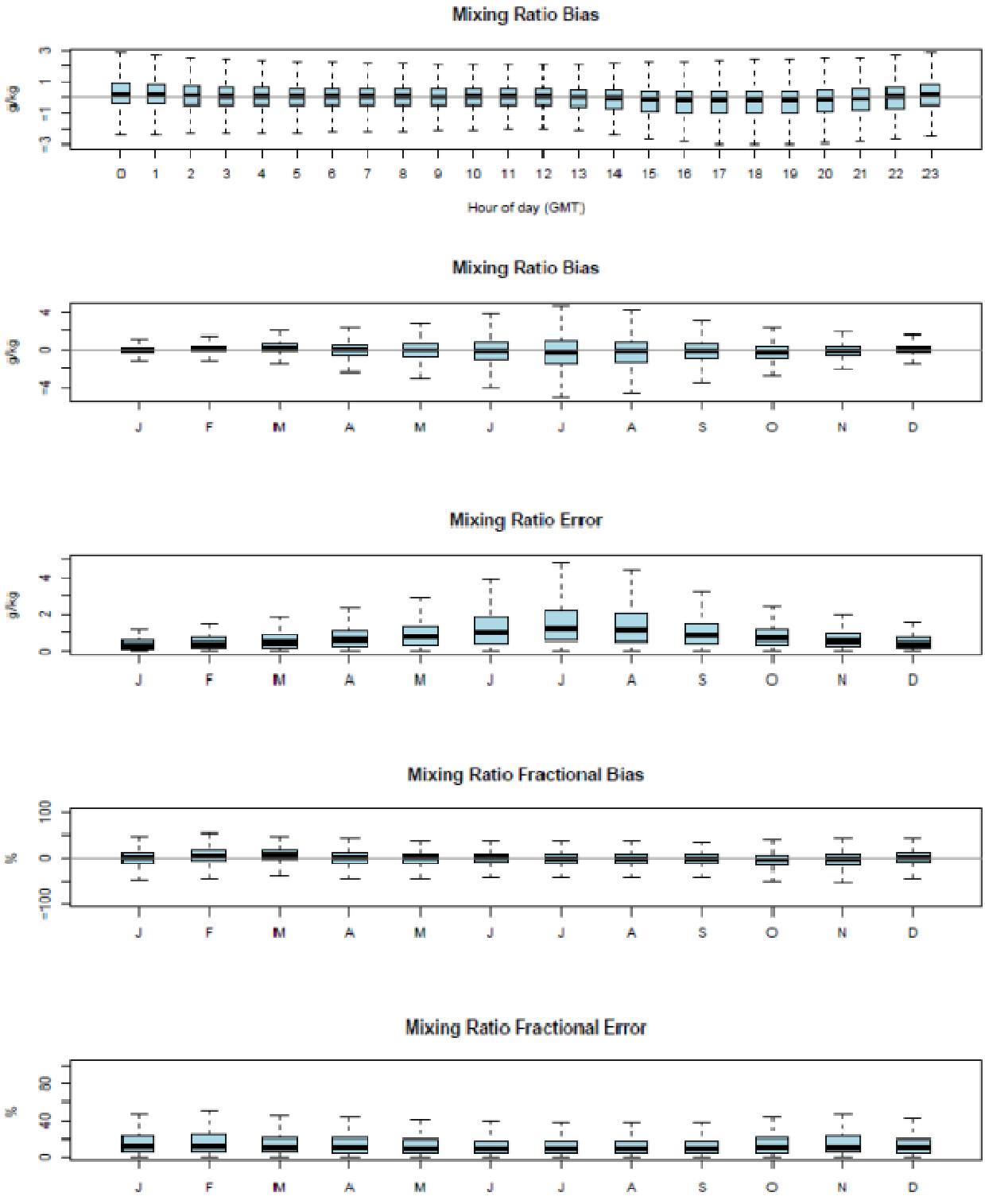

Figure 3.3.2. Distribution of hourly bias by hour and hourly bias, error, fractional bias, and fractional error for water vapor mixing ratio by month for the 12US2 domain.

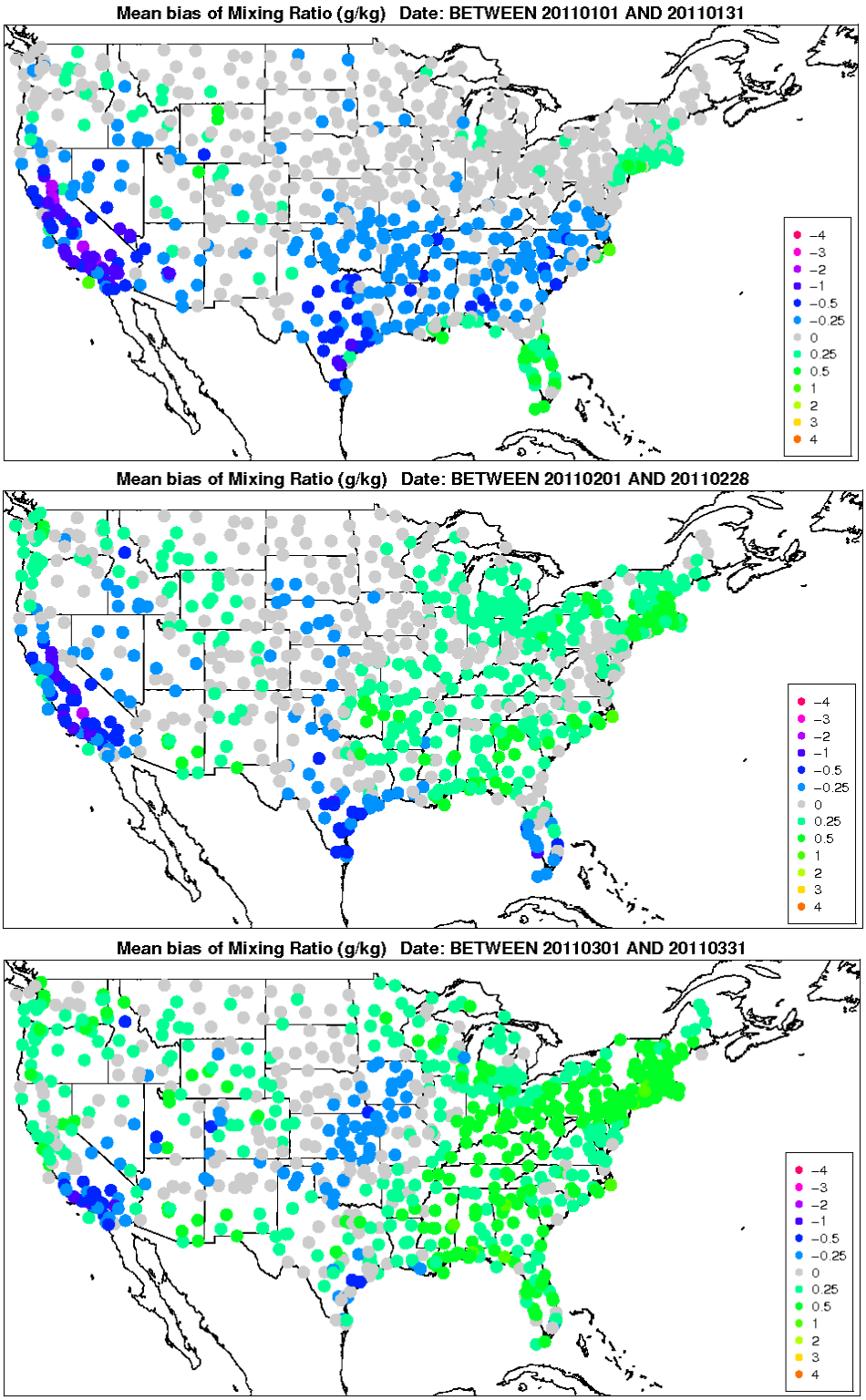

Figure 3.3.3. Spatial distribution of water vapor mixing ratio bias (g/kg) across all hours for the months of January, February, and March (top to bottom) for the 12US2 domain.

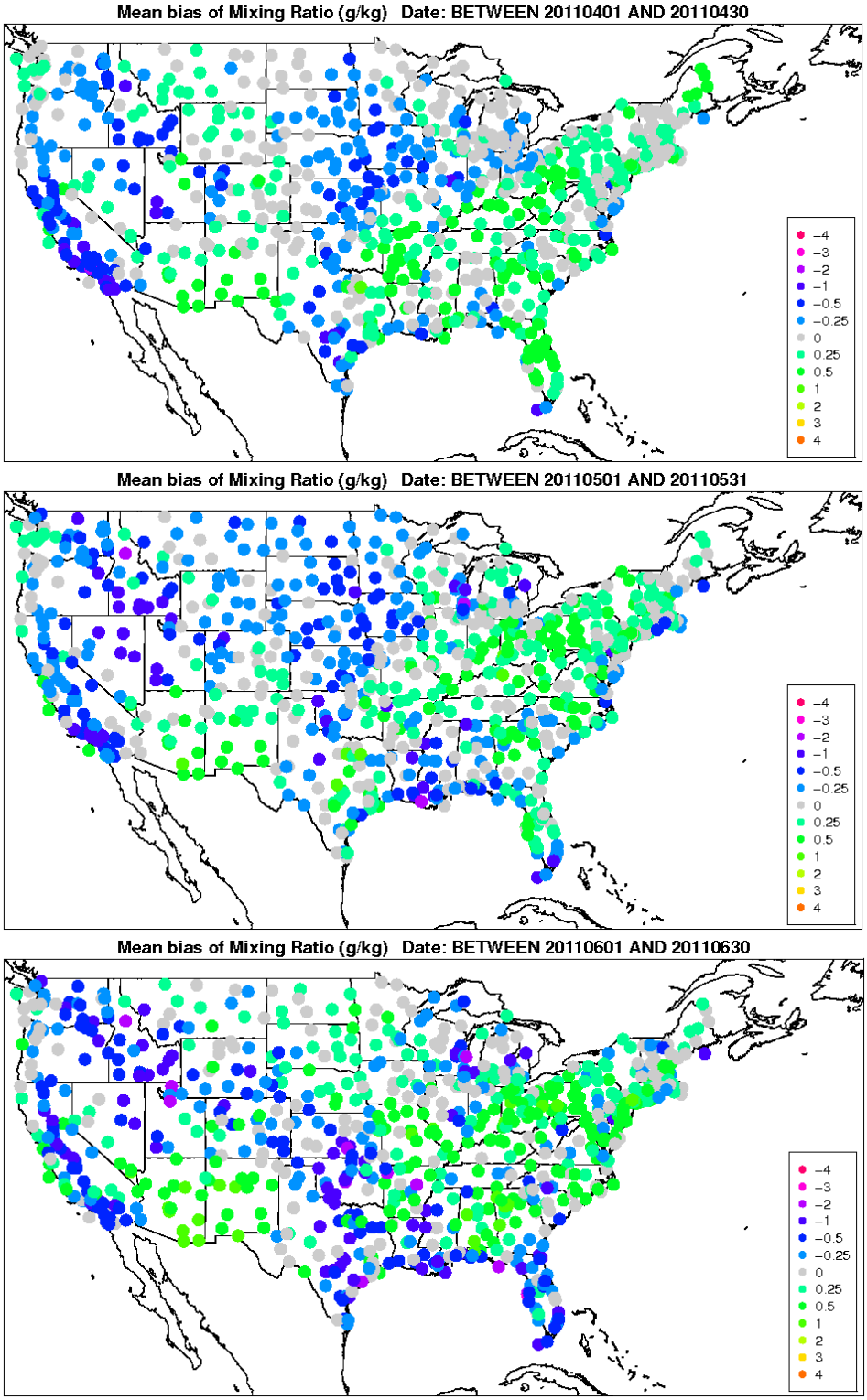

Figure 3.3.4. Spatial distribution of water vapor mixing ratio bias (g/kg) across all hours for the months of April, May, and June (top to bottom) for the 12US2 domain.

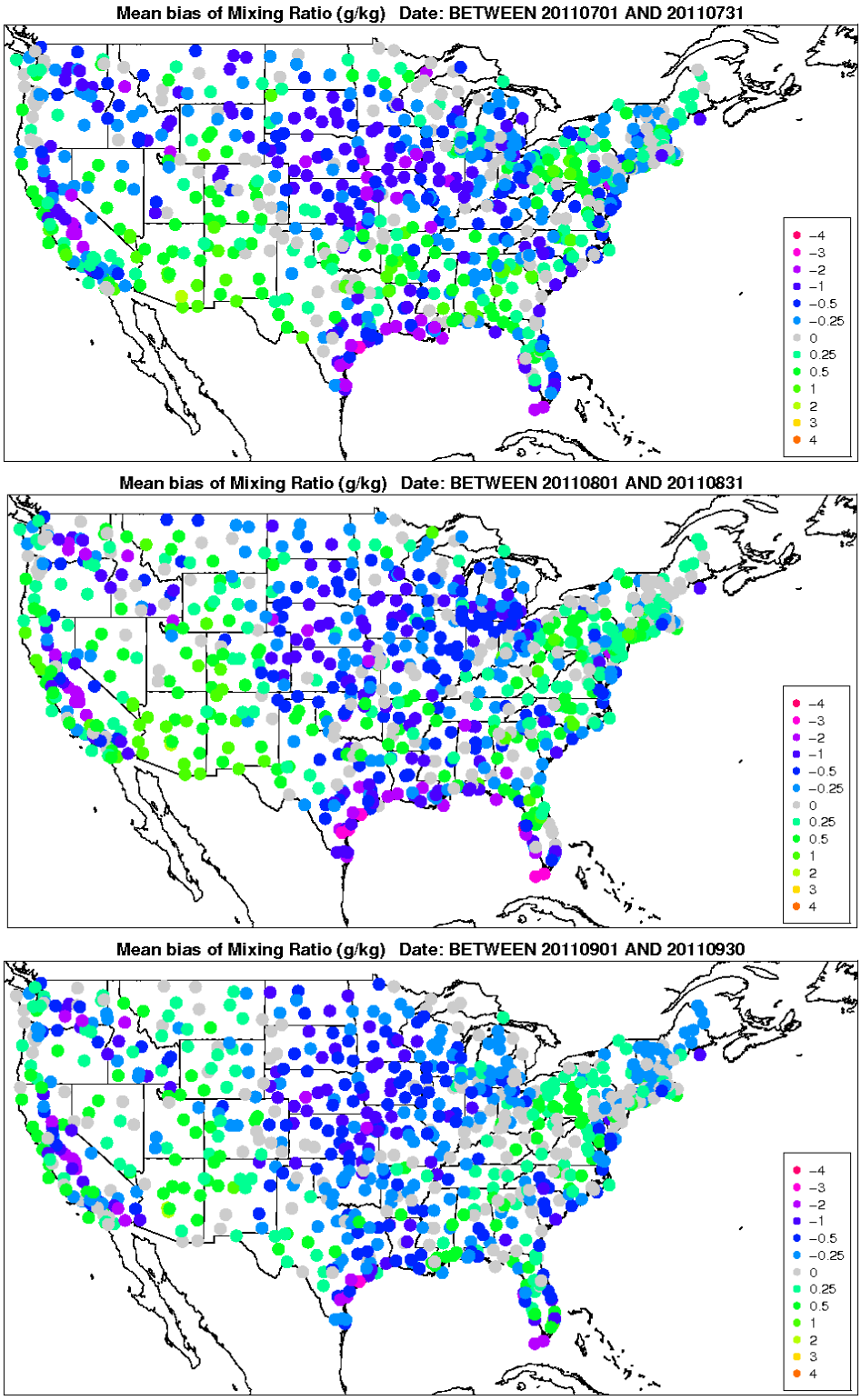

Figure 3.3.5. Spatial distribution of water vapor mixing ratio bias (g/kg) across all hours for the months of July, August, and September (top to bottom) for the 12US2 domain.

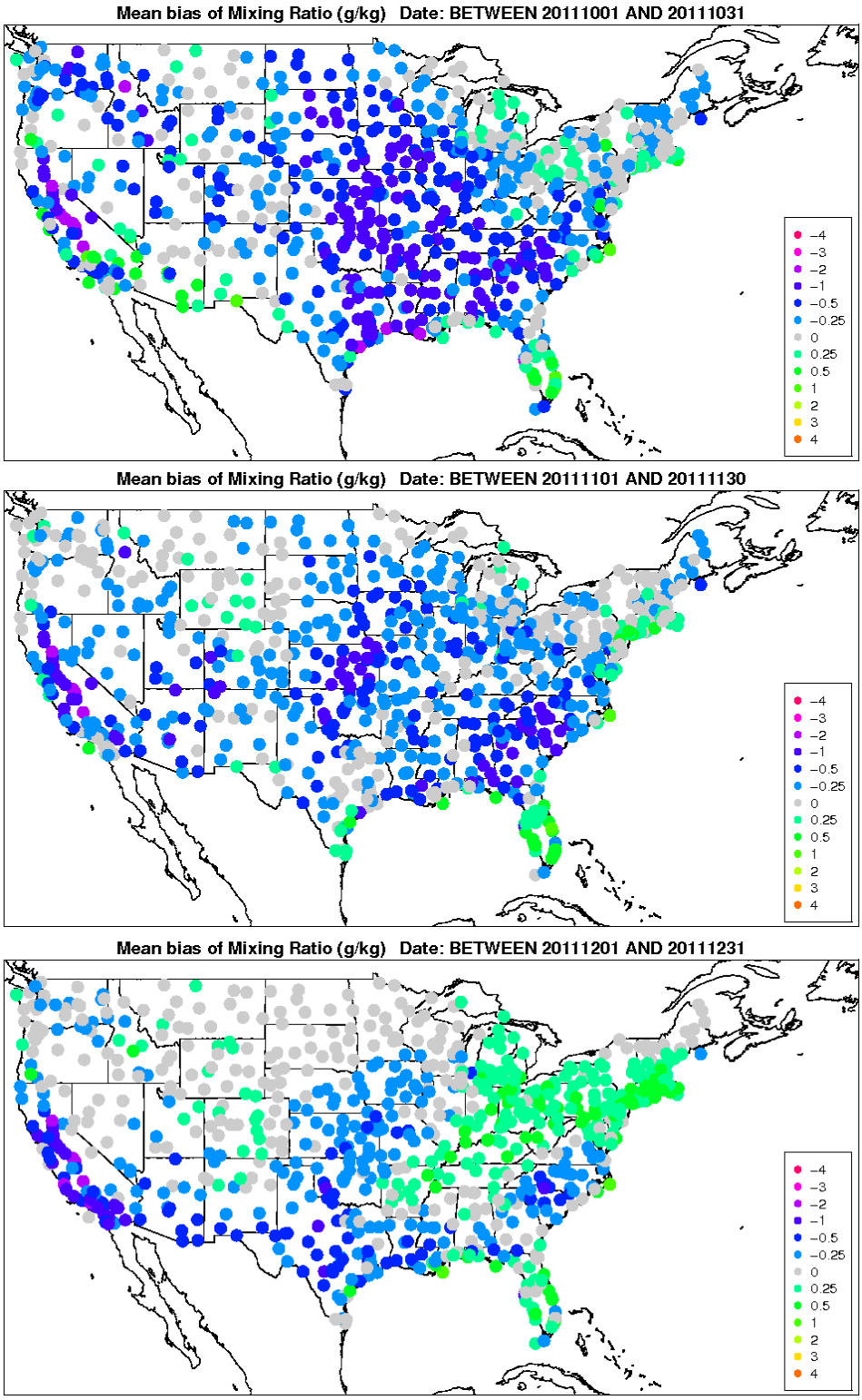

Figure 3.3.6. Spatial distribution of water vapor mixing ratio bias (g/kg) across all hours for the months of October, November, and December (top to bottom) for the 12US2 domain.

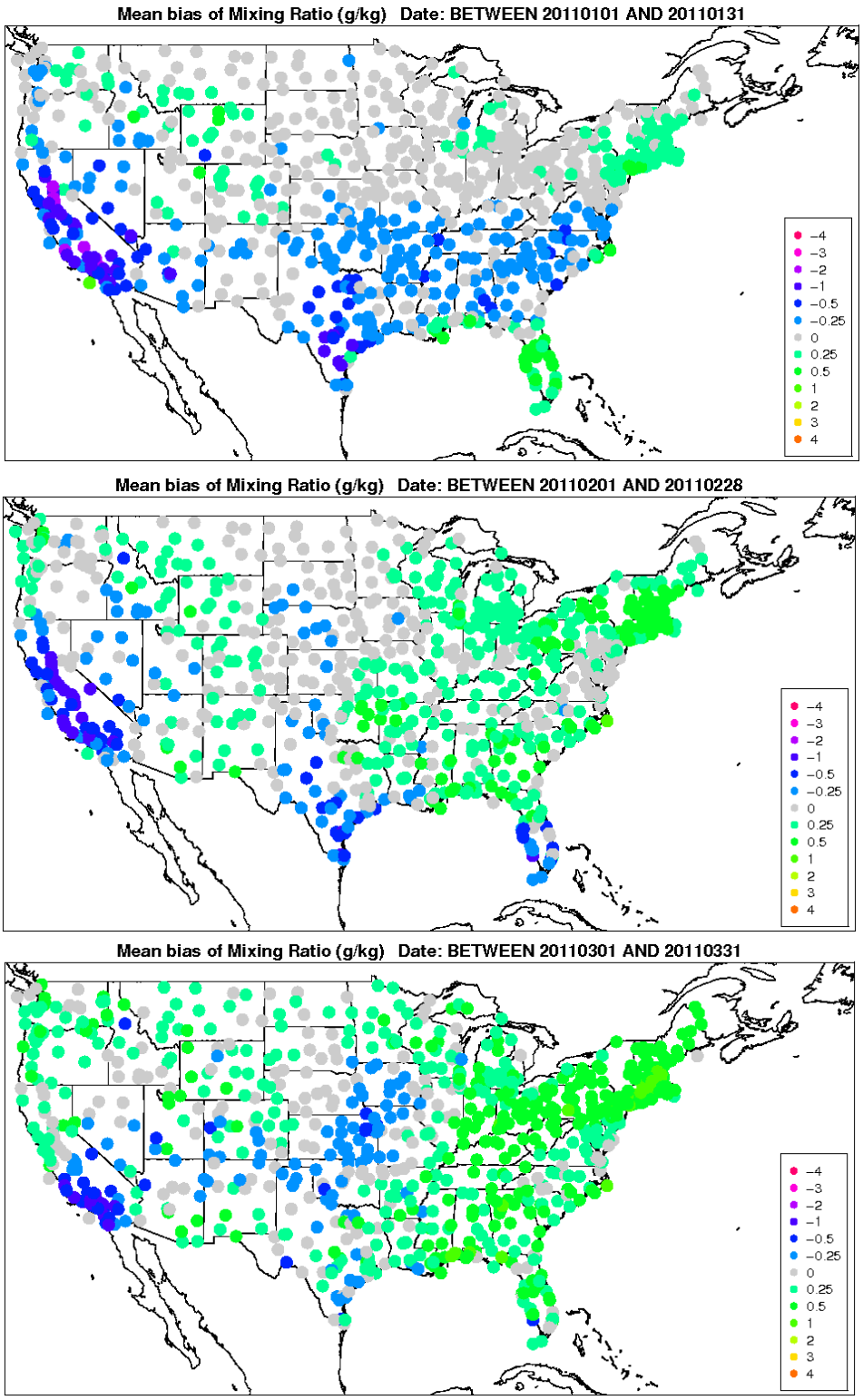

Figure 3.3.7. Spatial distribution of water vapor mixing ratio bias (g/kg) across daytime hours for the months of January, February, and March (top to bottom) for the 12US2 domain.

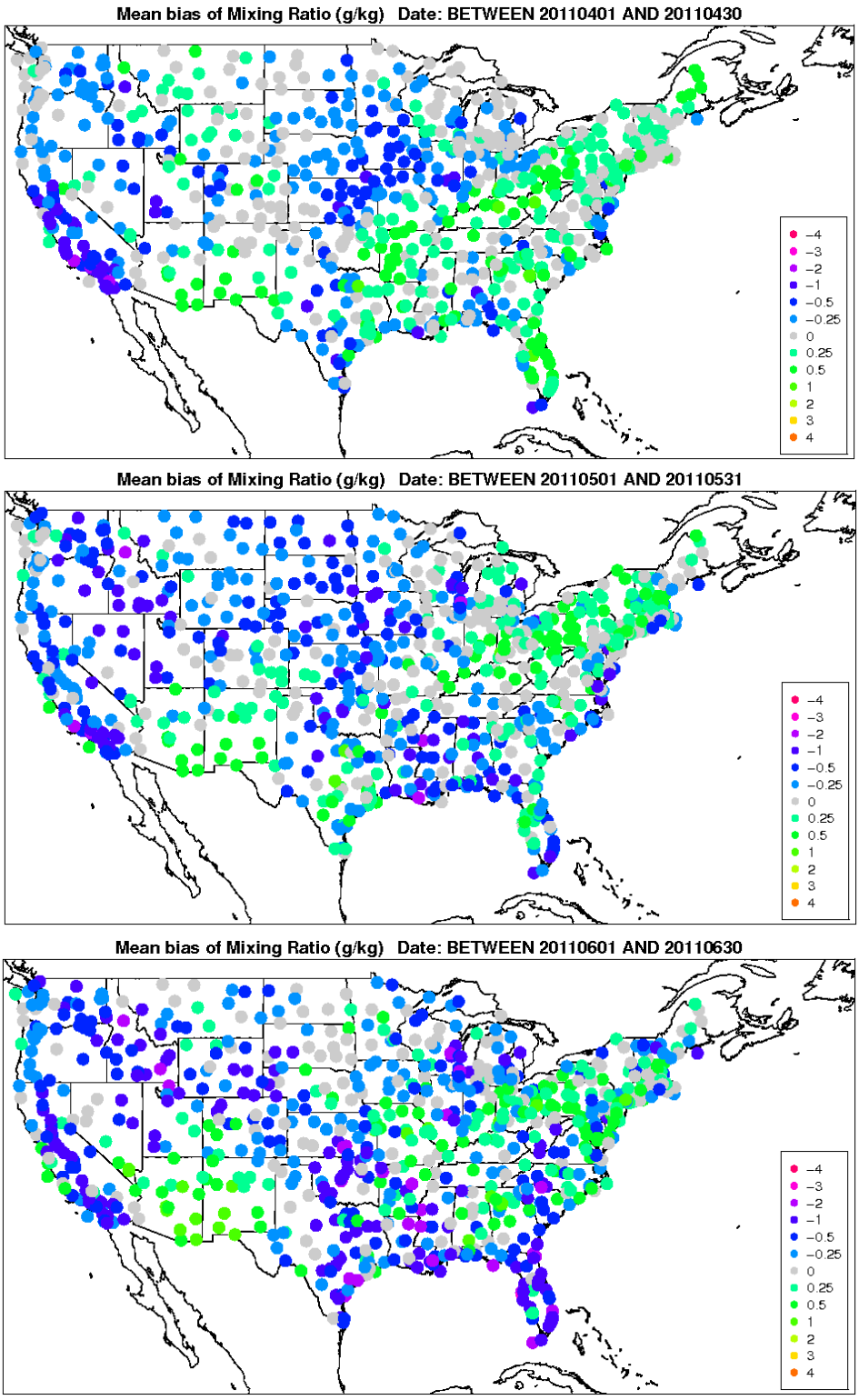

Figure 3.3.8. Spatial distribution of water vapor mixing ratio bias (g/kg) across daytime hours for the months of April, May, and June (top to bottom) for the 12US2 domain.

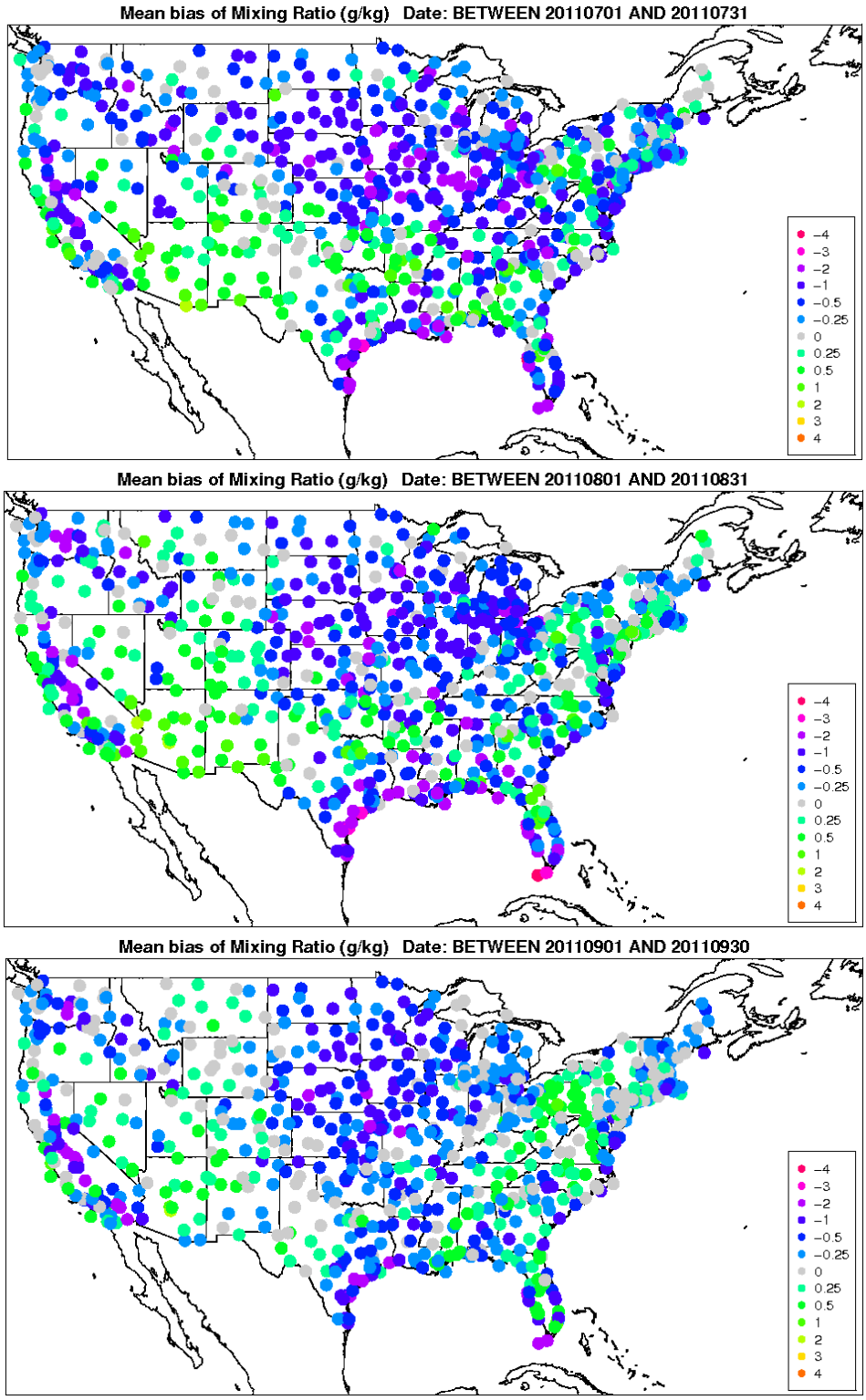

Figure 3.3.9. Spatial distribution of water vapor mixing ratio bias (g/kg) across daytime hours for the months of July, August, and September (top to bottom) for the 12US2 domain.

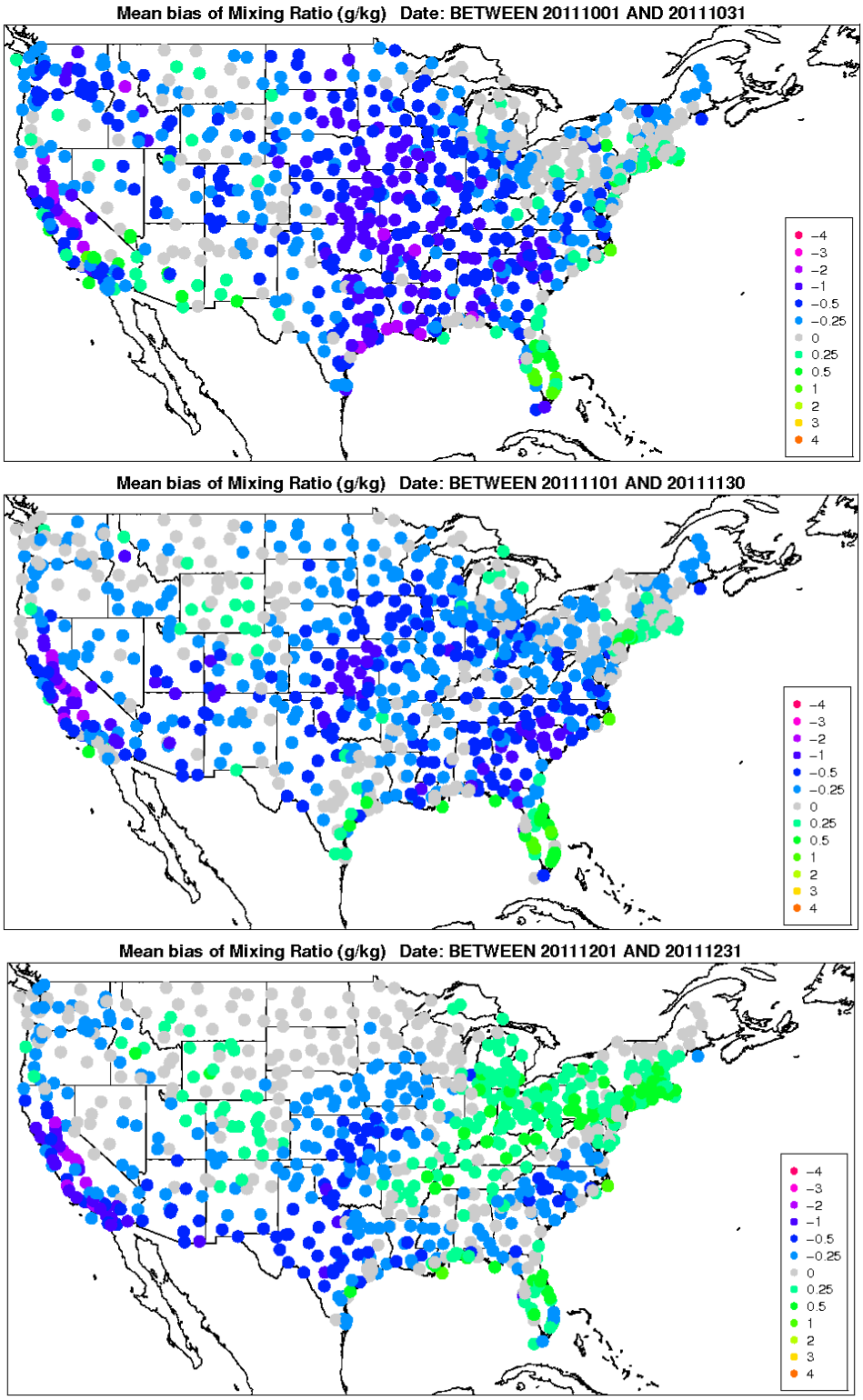

Figure 3.3.10. Spatial distribution of water vapor mixing ratio bias (g/kg) across daytime hours for the months of October, November, and December (top to bottom) for the 12US2 domain.

3.4 Precipitation

Monthly total rainfall is plotted for each grid cell to assess how well the model captures the spatial variability and magnitude of convective and non-convective rainfall. As described earlier, the PRISM estimations for rainfall are only within the continental United States. WRF rainfall estimates by month are shown for all grid cells in the domain. Monthly total estimates are shown for the 36US domain (Figures 3.4.1 through 3.4.4) and 12US2 domain (Figures 3.4.5 through 3.4.8).

In general, WRF performs adequately in terms of the spatial patterns and magnitude of precipitation across the US throughout the year. Both simulations, however, tend to overestimate precipitation in elevated terrain (e.g., northern CA and the Pacific Northwest). The 12km simulation tends to generate slightly higher precipitation amounts compared to the 36km simulation, and at times generates amounts higher than observed values (e.g., the southeast in July). Isolated amounts of overpredicted or underpredicted precipitation in the summer months relative to the observations is likely due to uncertainty in the convective parameterization scheme utilized.

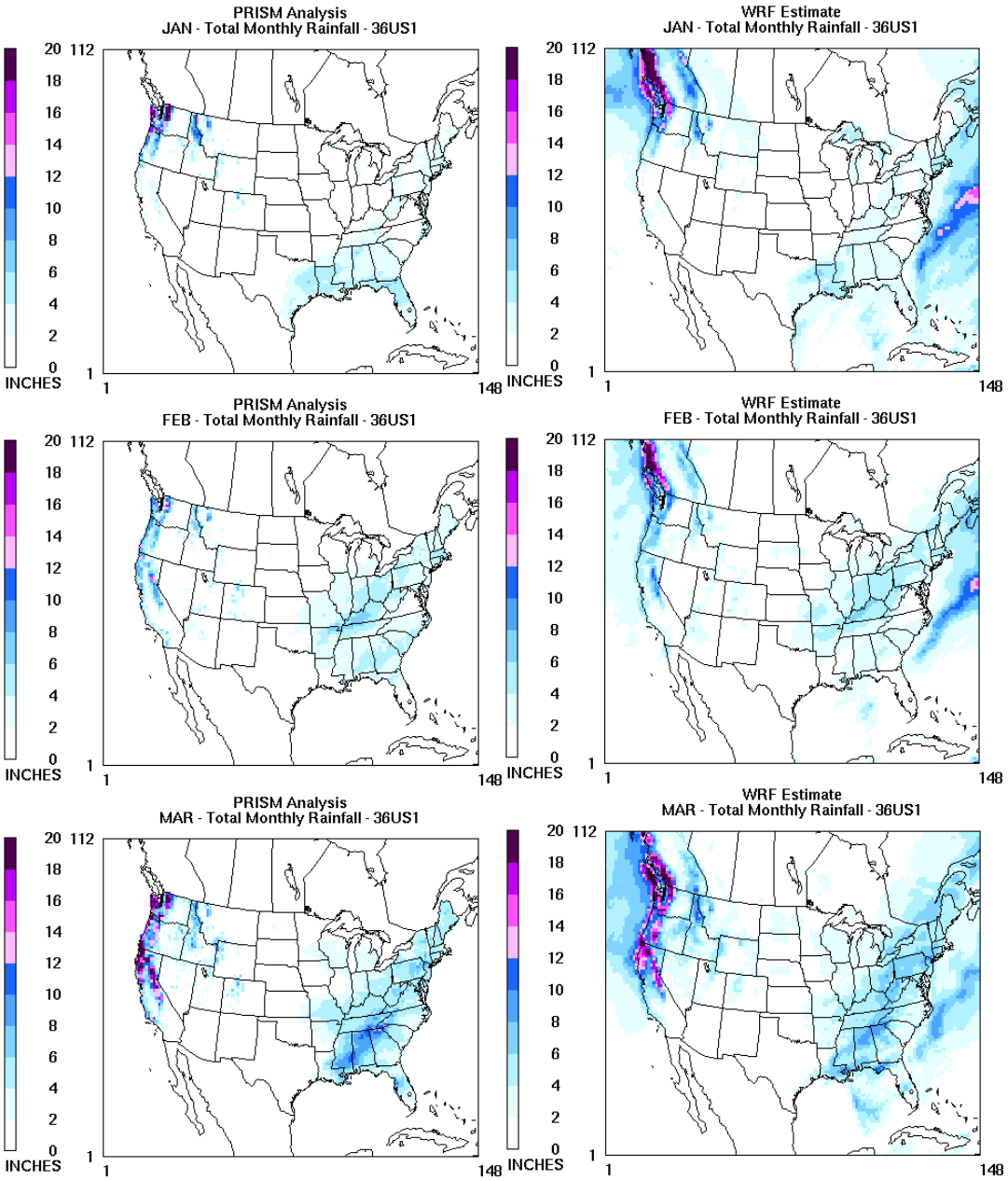

Figure 3.4.1. PRISM analysis (left) and WRF (right) estimated monthly total rainfall (in) for January, February, and March.

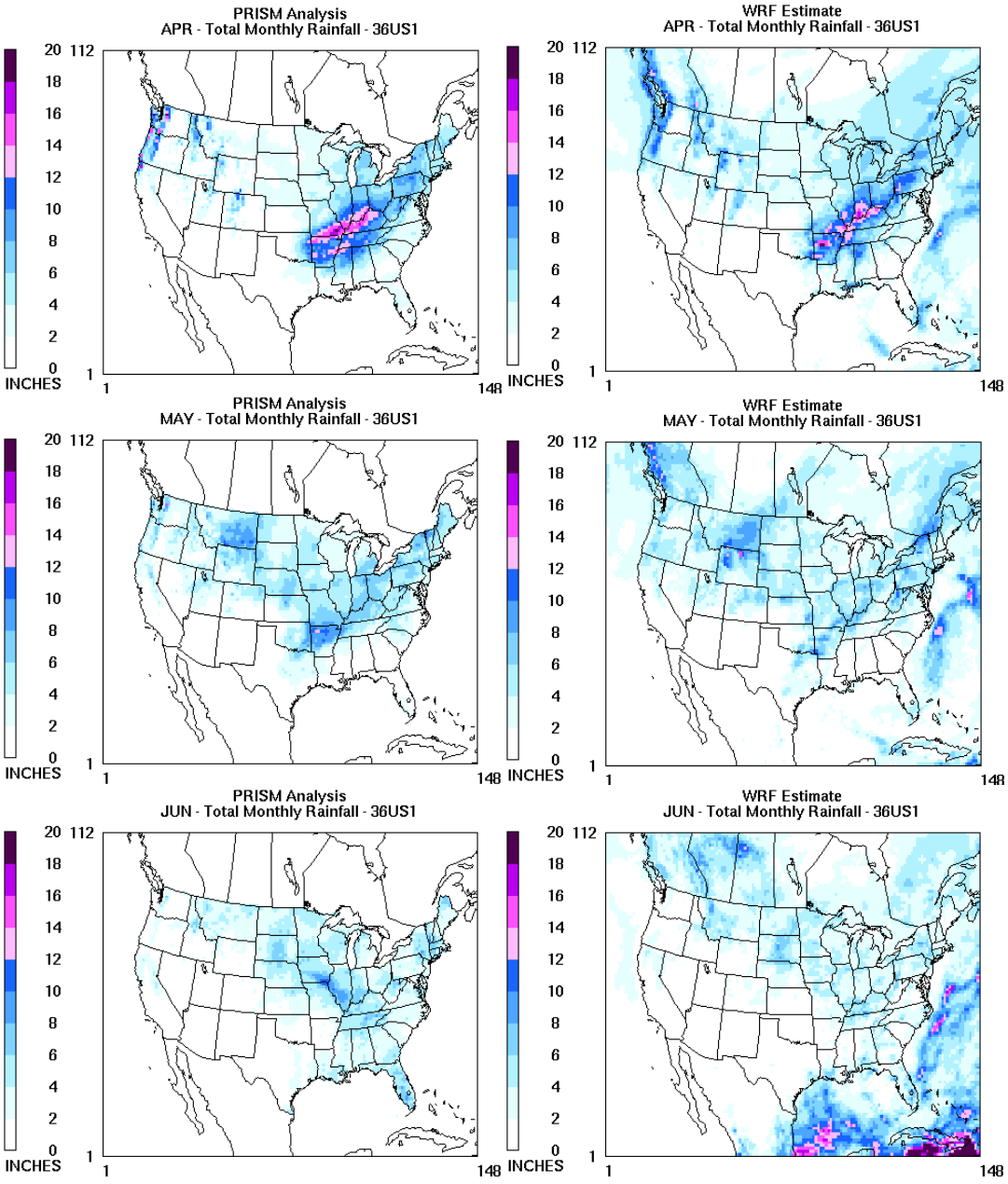

3.4.2. PRISM analysis (left) and WRF (right) estimated monthly total rainfall (in) for April, May, and June.

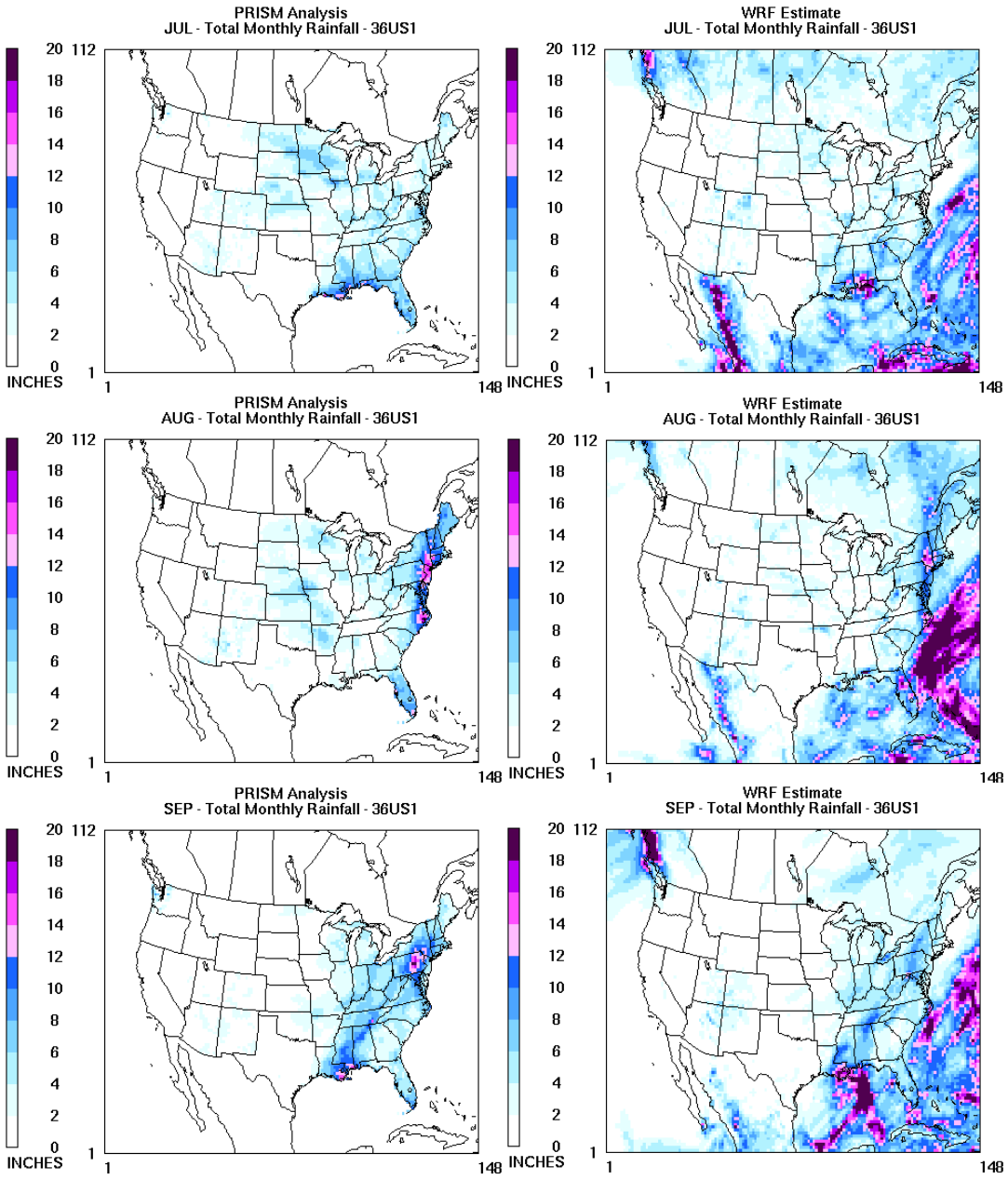

Figure 3.4.3. PRISM analysis (left) and WRF (right) estimated monthly total rainfall (in) for July, August, and September.

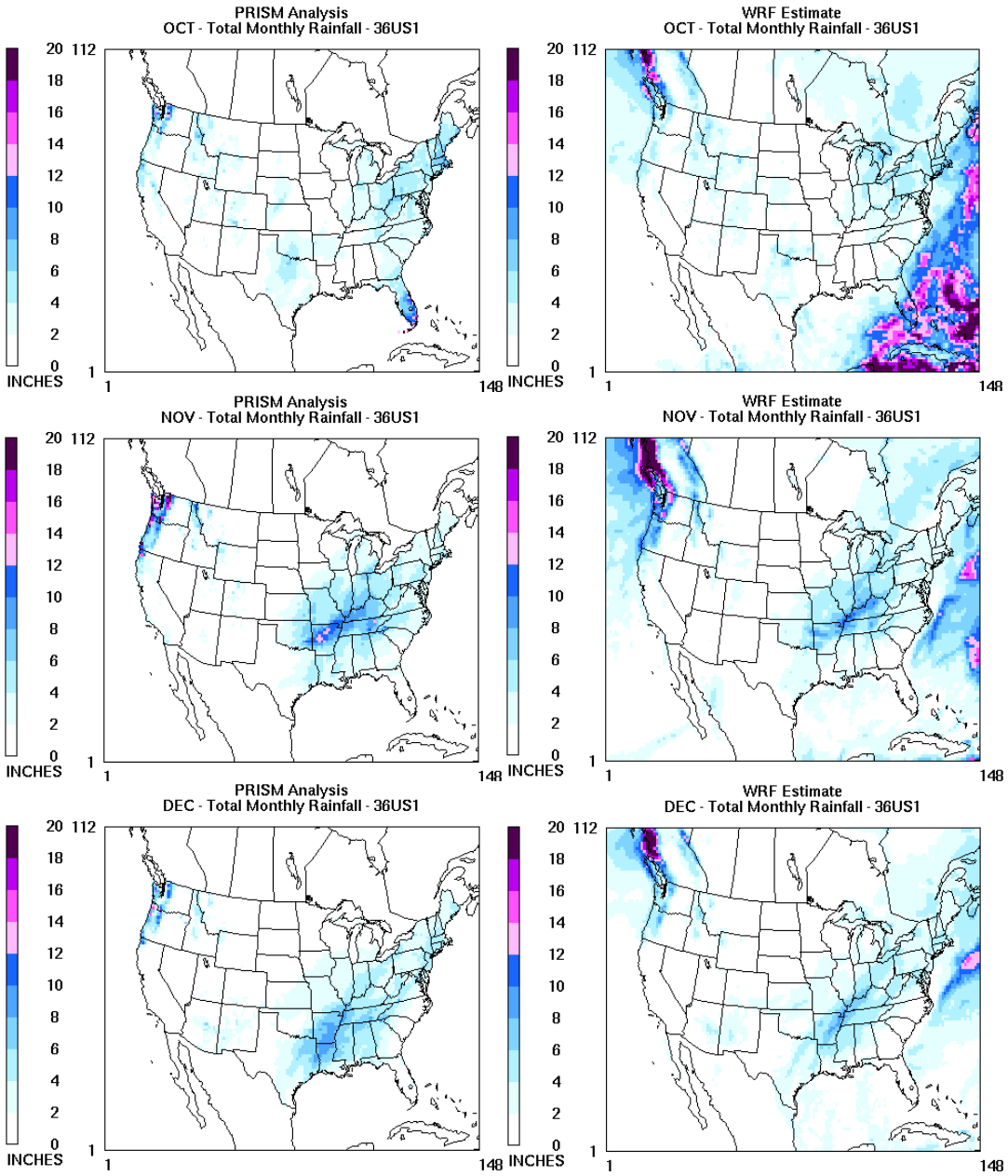

Figure 3.4.4. PRISM analysis (left) and WRF (right) estimated monthly total rainfall (in) for October, November, and December.

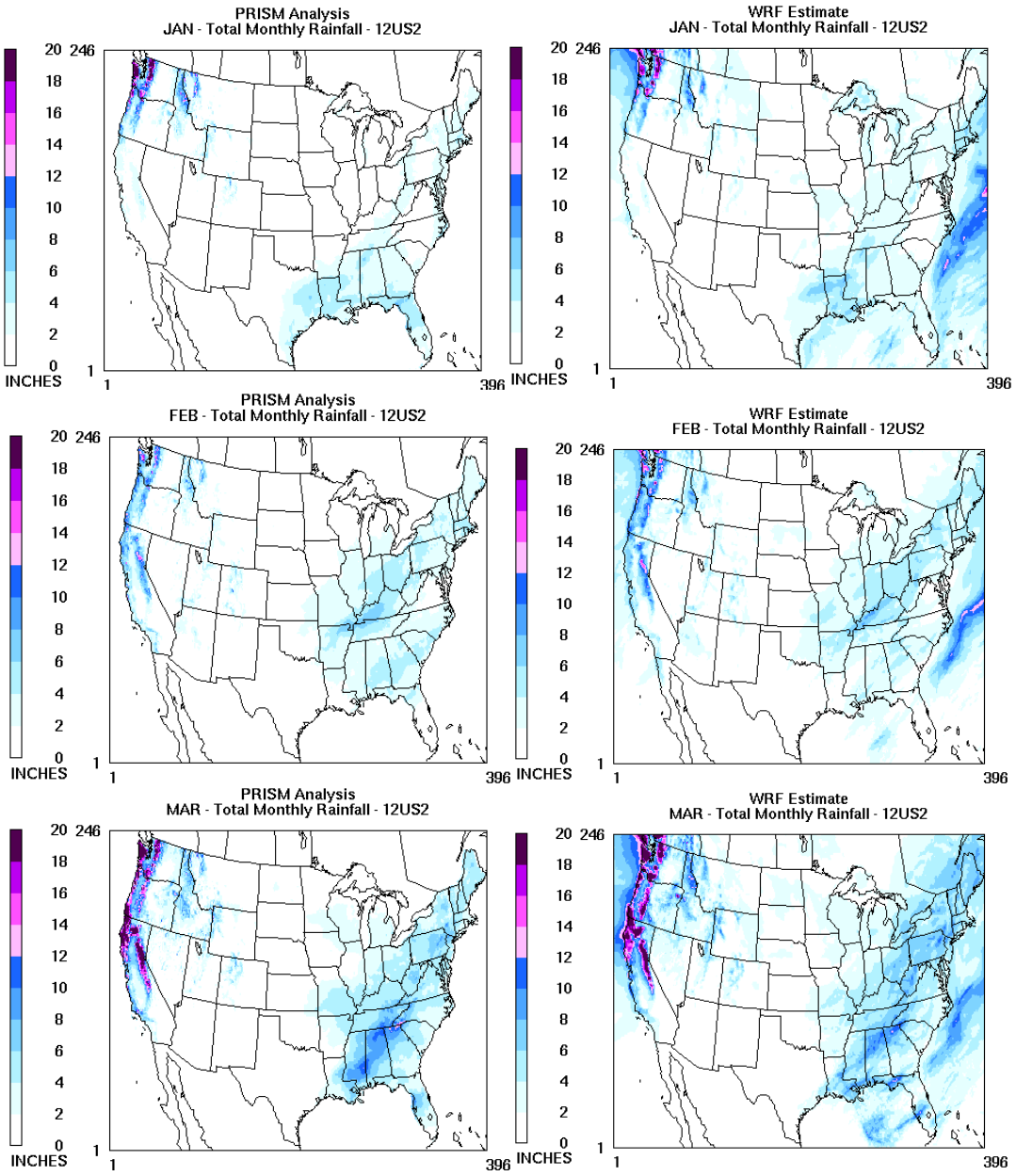

Figure 3.4.5. PRISM analysis (left) and WRF (right) estimated monthly total rainfall (in) for January, February, and March.

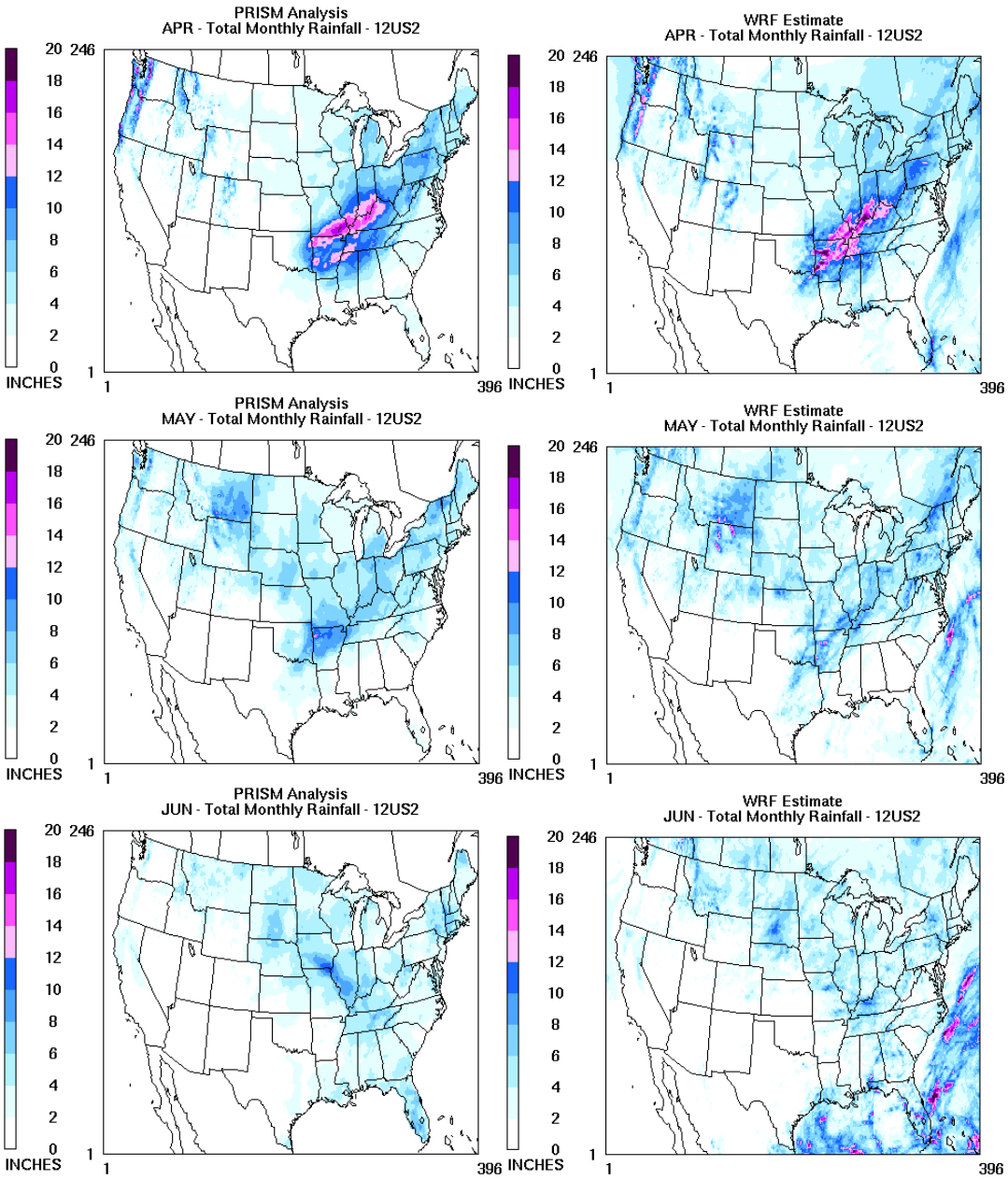

Figure 3.4.6. PRISM analysis (left) and WRF (right) estimated monthly total rainfall (in) for April, May, and June.

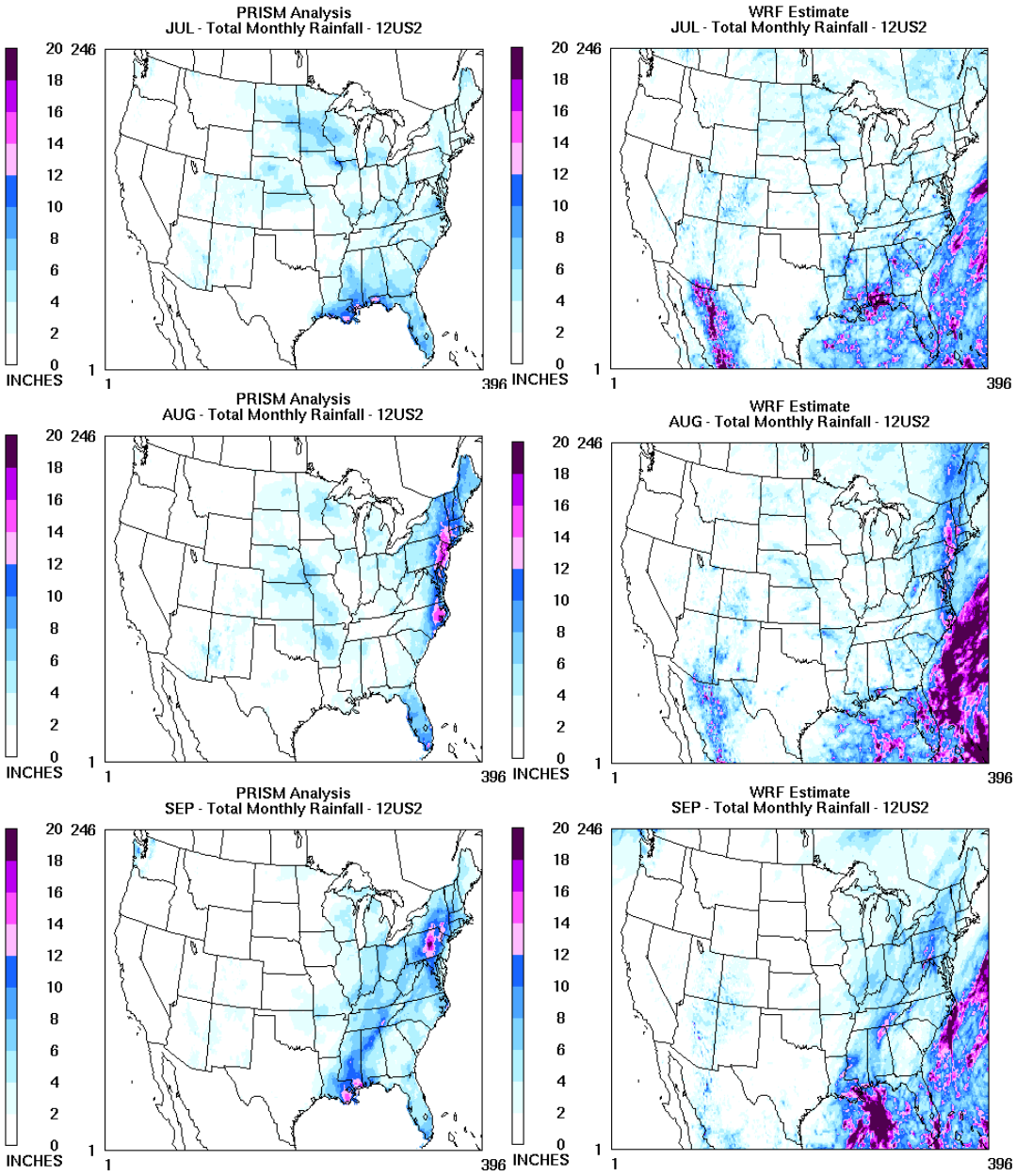

Figure 3.4.7. PRISM analysis (left) and WRF (right) estimated monthly total rainfall (in) for July, August, and September.

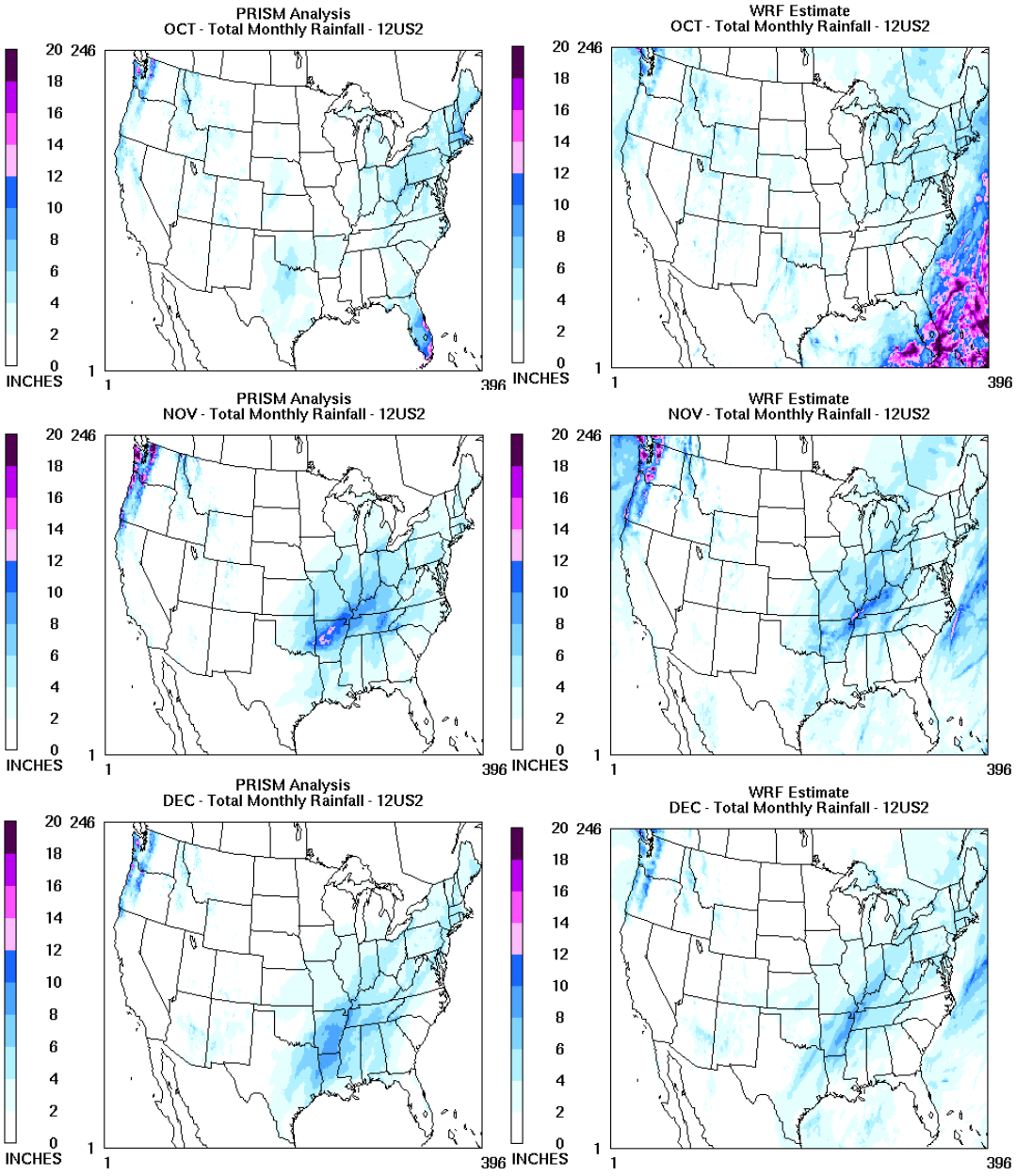

Figure 3.4.8. PRISM analysis (left) and WRF (right) estimated monthly total rainfall (in) for October, November, and December.

3.5 Solar Radiation

Photosynthetically activated radiation (PAR) is a fraction of shortwave downward radiation and is an important input for the biogenic emissions model for estimating isoprene (Carlton and Baker, 2011). Isoprene emissions are important for regional ozone chemistry and play a role in secondary organic aerosol formation. Radiation performance evaluation also gives an indirect assessment of how well the model captures cloud formation during daylight hours.

Shortwave downward radiation estimates are compared to surface based measurements made at SURFRAD and ISIS network monitors for the 36US (Figure 3.6.1) 12US2 (Figure 3.6.2) domains.

Overall, both the 36- and 12km simulations show WRF has little bias in shortwave radiation predictions during the fall and winter months. Biases tend to grow during the spring and peak in the summer, though the spread in overpredictions tends to be less than 100 W/m^2 on average, with a median bias close to zero.

More variability is noted on an hourly basis. WRF tends to overpredict early morning to early afternoon shortwave radiation, while underpredicting the late afternoon and early evening values. The median overprediction at the time of greatest incoming solar radiation is near 100 W/m^2. In the late afternoon and evening hours, the median bias is close to -50 W/m^2. These errors are likely attributable to the model being unable to accurately simulate cloud features at subgrid (<12km) scales. This assumption is based on the slight improvement in predictions at 12km versus 36km.

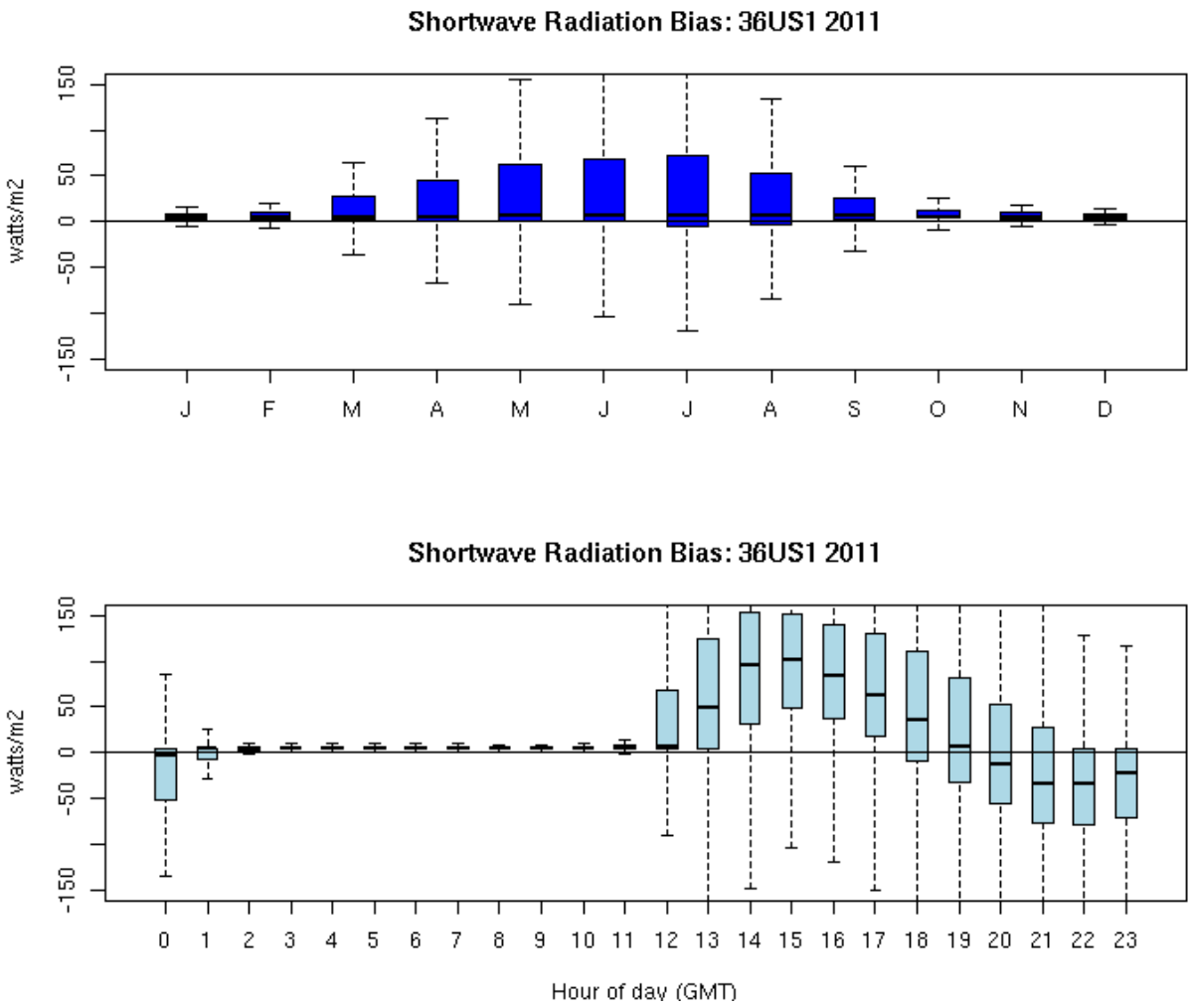

Figure 3.5.1. Distribution of hourly bias for shortwave radiation (W/m^2) by month (top) and by hour of the day (bottom) for the 36US domain.

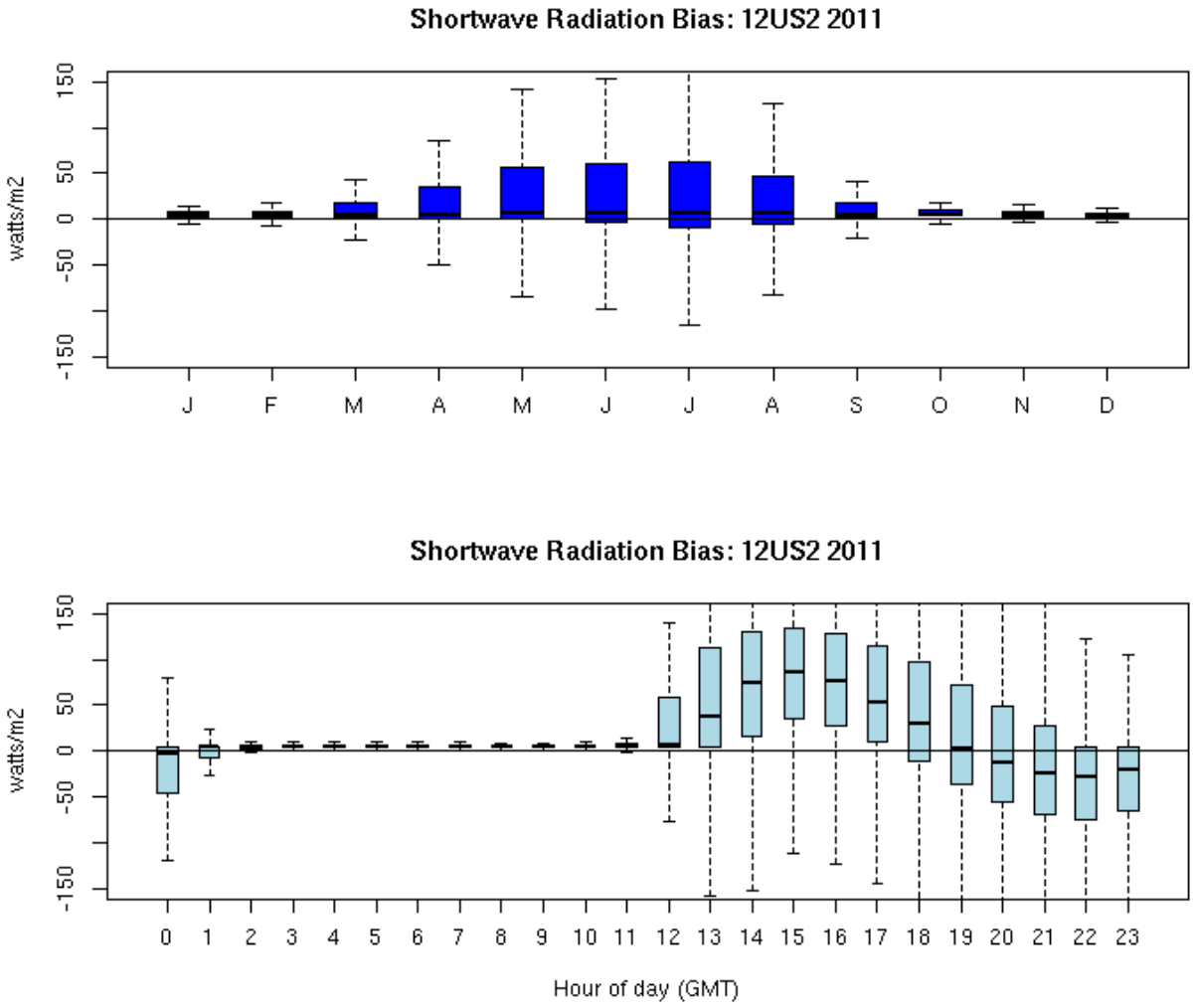

Figure 3.5.2. Distribution of hourly bias for shortwave radiation (W/m^2) by month (top) and by hour of the day (bottom) for the 12US2 domain.

4 CLIMATE REPRESENTATIVENESS OF 2011

Figures 4.1 and 4.2 show the divisional rankings for observed temperatures across the US for 2011. A climatic representation of the precipitation for 2011 is shown in Figures 4.3 and 4.4. These plots are useful in determining the representativeness of 2011 in terms of certain climatological variables compared to historical averages.

Temperatures in 2011 were average to above average for most of the central and eastern US throughout the spring and summer months. Some areas in the southern and southeastern portions of the country exhibited near record warmth from June through August. Conversely, February through July tended to be cooler than average for the western US with near-record cold exhibited in the Pacific Northwest.

The spring and summer months experienced below average precipitation for much of the southern and southeastern US, whereas wetter conditions than average were experienced across the northern tier states. During the fall and winter months, most of the eastern US experienced average to above average precipitation, while the western and southern US remained generally below average.

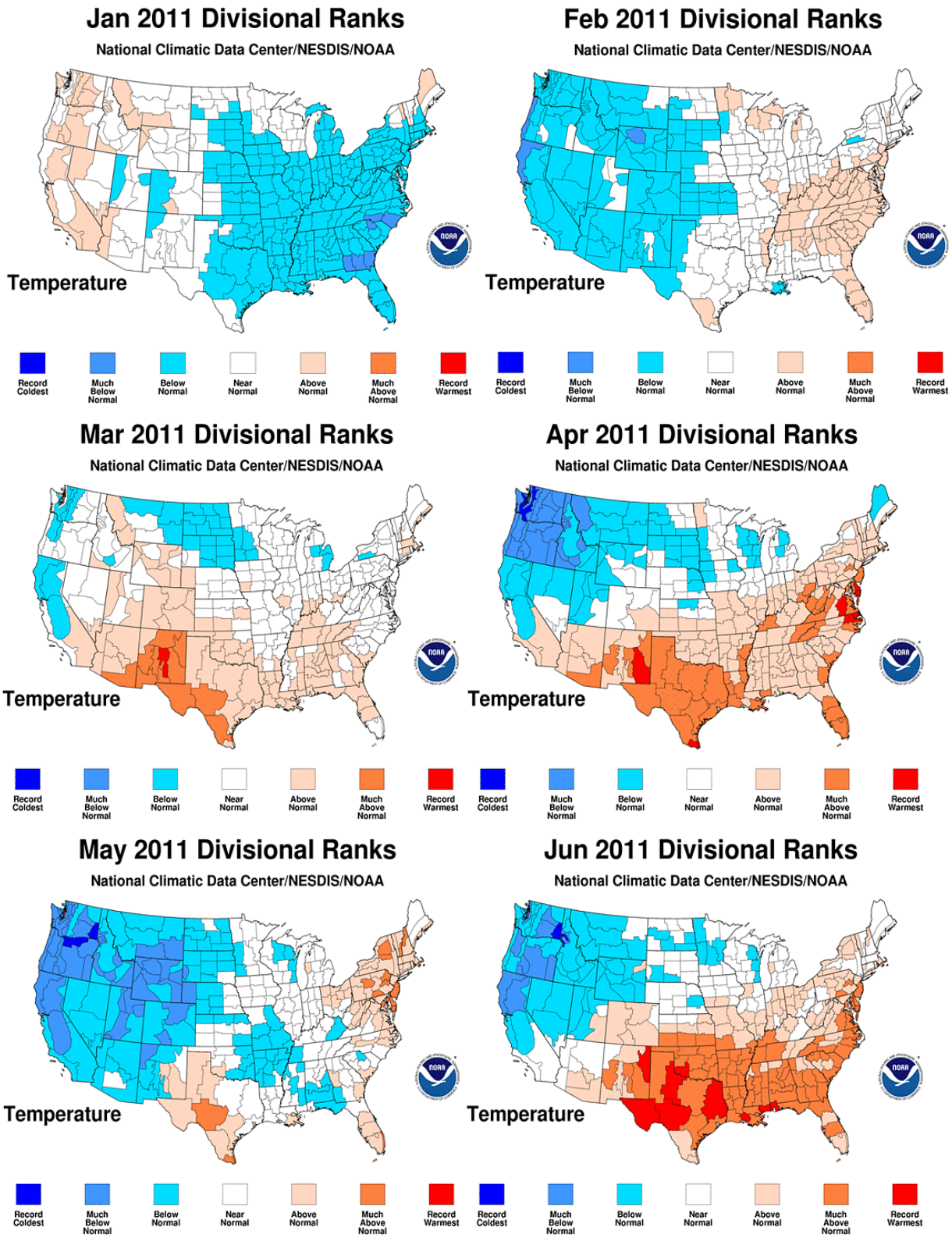

Figure 4.1 Climatic temperature rankings by climate division: January to June 2011. http://www.ncdc.noaa.gov/temp-and-precip/maps.php

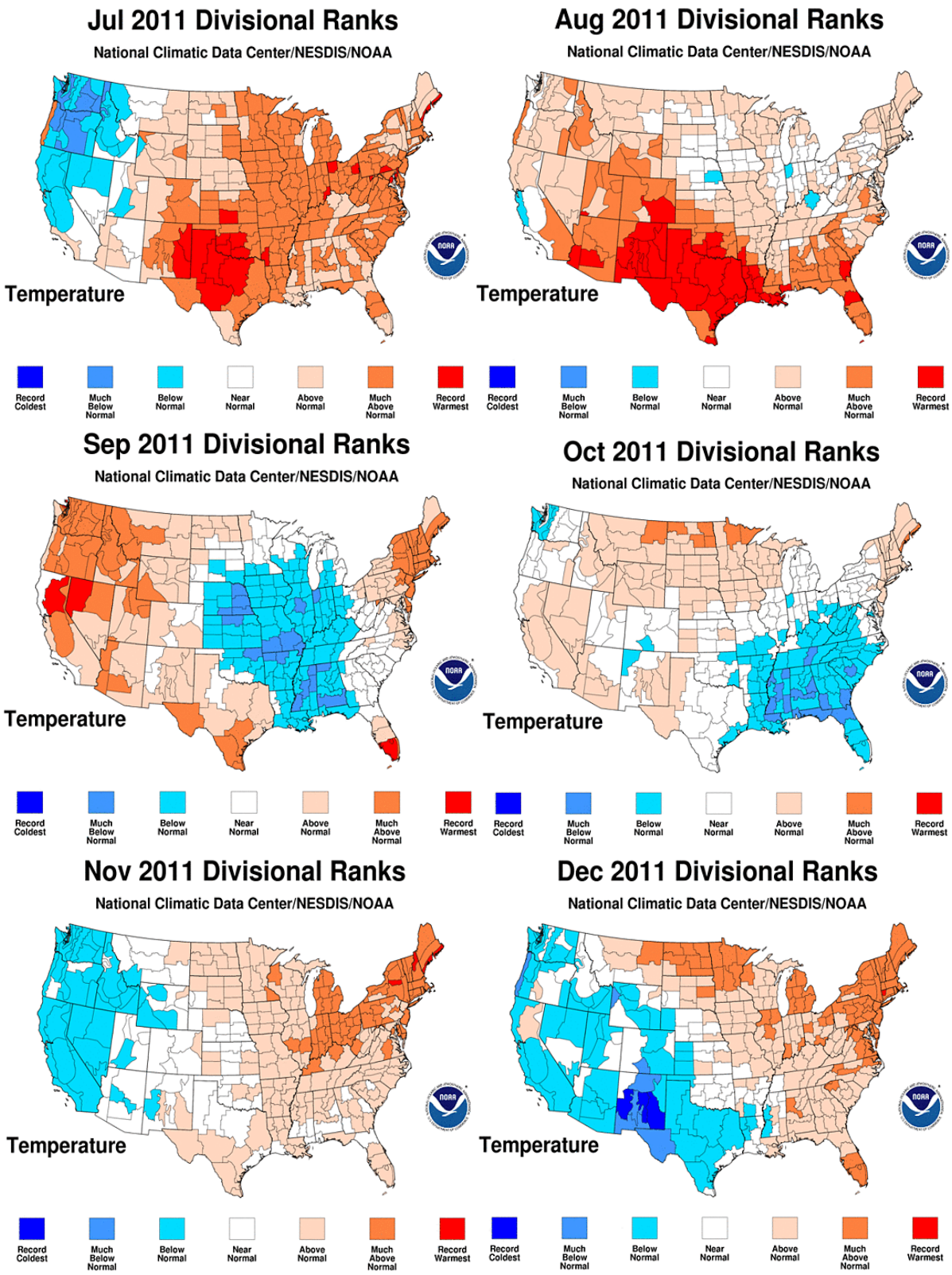

Figure 4.2 Climatic temperature rankings by climate division: July to December 2011. http://www.ncdc.noaa.gov/temp-and-precip/maps.php

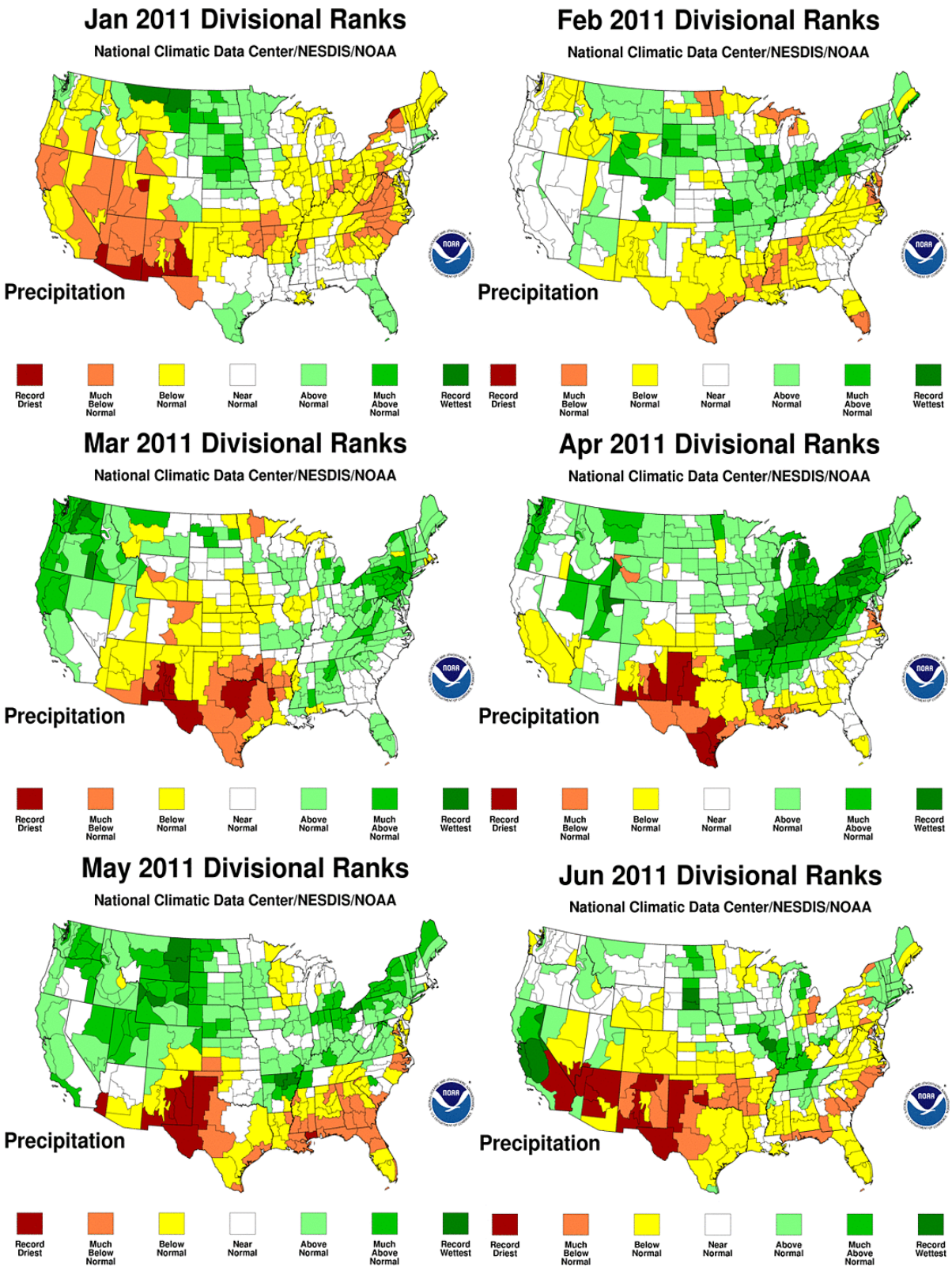

Figure 4.3 Climatic rainfall rankings by climate division: January to June 2011. http://www.ncdc.noaa.gov/temp-and-precip/maps.php

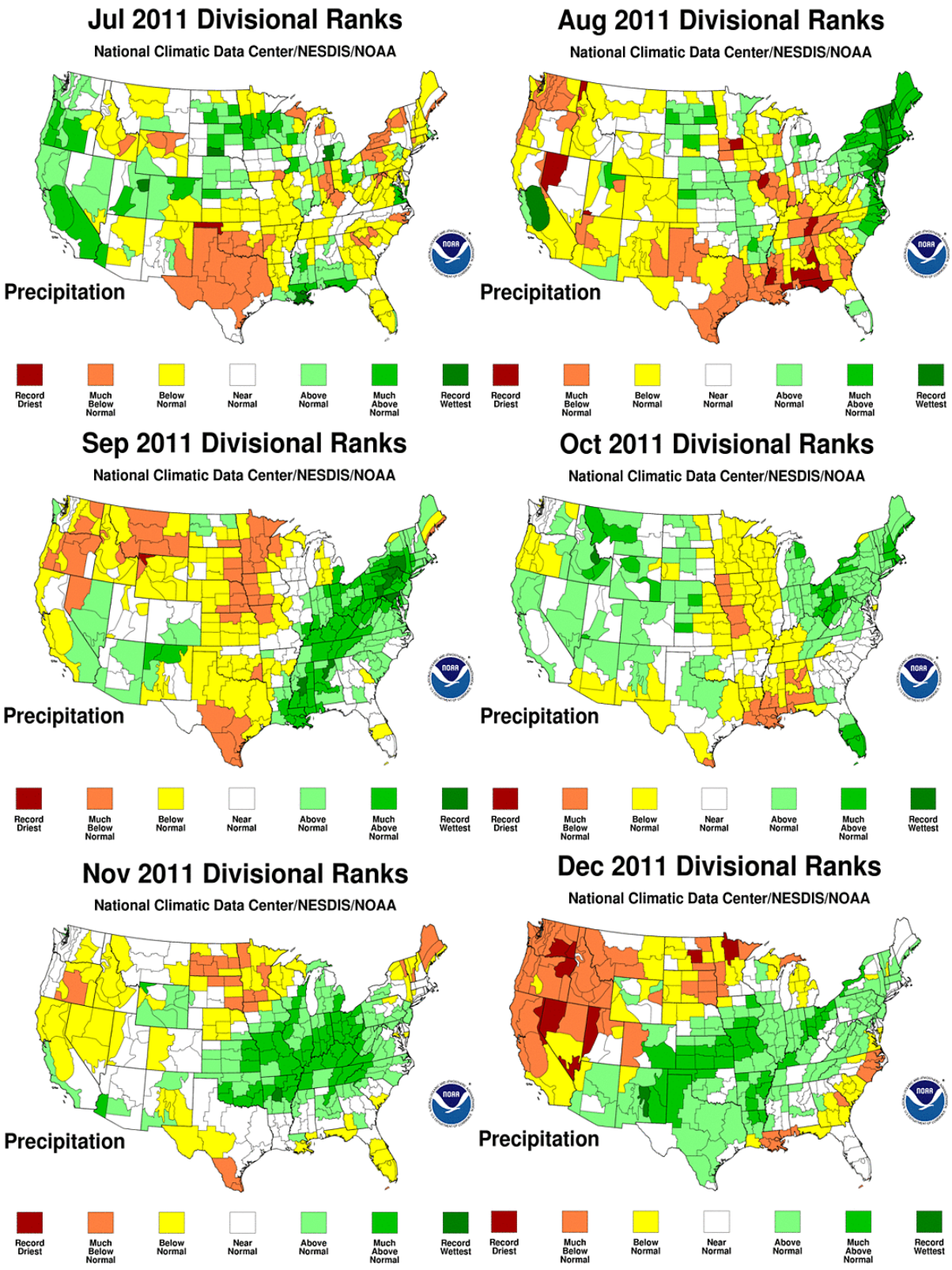

Figure 4.4 Climatic rainfall rankings by climate division: July to December 2011. http://www.ncdc.noaa.gov/temp-and-precip/maps.php

5 REFERENCES

Boylan, J.W., Russell, A.G., 2006. PM and light extinction model performance metrics, goals, and criteria for three-dimensional air quality models. Atmospheric Environment 40, 4946-4959.

Carlton, A.G., Baker, K.R., 2011. Photochemical Modeling of the Ozark Isoprene Volcano: MEGAN, BEIS, and Their Impacts on Air Quality Predictions. Environmental Science & Technology 45, 4438-4445.

Cooper, O.R., Stohl, A., Hubler, G., Hsie, E.Y., Parrish, D.D., Tuck, A.F., Kiladis, G.N., Oltmans, S.J., Johnson, B.J., Shapiro, M., Moody, J.L., Lefohn, A.S., 2005. Direct Transport of Midlatitude Stratospheric Ozone into the Lower Troposphere and Marine Boundary Layer of the Pacific Ocean. Journal of Geophysical Research – Atmospheres 110, D23310, doi:10.1029/2005JD005783.

ENVIRON, 2008. User's Guide Comprehensive Air Quality Model with Extensions. ENVIRON International Corporation, Novato.

Gilliam, R.C., Pleim, J.E., 2010. Performance Assessment of New Land Surface and Planetary Boundary Layer Physics in the WRF-ARW. Journal of Applied Meteorology and Climatology 49, 760-774.

Langford, A.O., Reid, S.J., 1998. Dissipation and Mixing of a Small-Scale Stratospheric Intrusion in the Upper Troposphere. Journal of Geophysical Research 103, 31265-31276.

Otte, T.L., Pleim, J.E., 2010. The Meteorology-Chemistry Interface Processor (MCIP) for the CMAQ modeling system: updates through MCIPv3.4.1. Geoscientific Model Development 3, 243-256.

Skamarock, W.C., Klemp, J.B., Dudhia, J., Gill, D.O., Barker, D.M., Duda, M.G., Huang, X., Wang, W., Powers, J.G., 2008. A Description of the Advanced Research WRF Version 3.

Stammer, D., F.J. Wentz, and C.L. Gentemann, 2003, Validation of Microwave Sea Surface Temperature Measurements for Climate Purposes, *J. Climate,* 16, 73-87.